FORMATION ESTABLISHMENT AND RECONFIGURATION USING DIFFERENTIAL ELEMENTS IN J2-PERTURBED ORBITS

C. W. T. Roscoe, J. J. Westphal, J. D. Griesback and Hanspeter Schaub

IEEE Aerospace Conference

Big Sky, Montana **March 1–8, 2014**

Formation Establishment and Reconfiguration Using Differential Elements in J2-Perturbed Orbits

Christopher W. T. Roscoe
Applied Defense Solutions
Columbia, MD 21044
410-715-0005
CRoscoe@applieddefense.com

Jason J. Westphal
Applied Defense Solutions
Columbia, MD 21044
410-715-0005
JWestphal@applieddefense.com

Jacob D. Griesbach
Applied Defense Solutions
Columbia, MD 21044
410-715-0005
JGriesbach@applieddefense.com

Hanspeter Schaub
Applied Defense Solutions
Columbia, MD 21044
410-715-0005
HSchaub@applieddefense.com

***Abstract*—A practical algorithm is developed for on-board planning of n-impulse fuel-optimal maneuvers for establishment and reconfiguration of spacecraft formations. The method is valid in circular and elliptic orbits and includes first-order secular J_2 effects. The dynamics are expressed in terms of differential mean orbital elements, and relations are provided to allow the formation designer to transform these into intuitive geometric quantities for visualization and analysis. The maneuver targeting problem is formulated as an optimal control problem in both continuous and discrete time. The continuous-time formulation cannot be solved directly in an efficient manner, and the discrete-time formulation, which has an analytical solution, does not directly yield the optimal thrust times. Therefore, a practical algorithm is designed by iteratively solving the discrete-time formulation while using the continuous-time necessary conditions to refine the thrust times until they converge to the optimal values. Simulation results are shown for a variety of reconfiguration maneuvers and reference orbits, including simulations with and without navigation errors for the NASA CubeSat Proximity Operations Demonstration mission.**

TABLE OF CONTENTS

1. INTRODUCTION

Spacecraft formation flying is a key area of research in modern spacecraft dynamics and control. Numerous formation flying missions have been conceived over the past two decades and many have flown successfully. This concept enables several mission types including sparse apertures, where multiple spacecraft take the place of a large antenna or telescope, magnetic and electrical interaction studies, and on-orbit servicing or inspection. One important area of research in this field is the development of algorithms for establishing or reconfiguring a formation.

Formation establishment or reconfiguration is defined as the process of taking a spacecraft formation from some initial configuration and transforming it to another configuration. This is necessary in order to, for example, establish a synthetic aperture, initiate or change proximity operations trajectories for inspection of a debris object, or recover from a period of uncontrolled drift. The main problem addressed in this paper is that of designing maneuvers, made up of n impulsive thrusts, to take a spacecraft formation from some initial trajectory to a desired trajectory with as little fuel as possible.

This is by no means a new problem and it has been investigated by numerous authors in the past. However, the previous methods suffer from one or more of the following drawbacks:

1. They involve the computationally expensive and sensitive solution of sets of nonlinear equations [1–13].
2. They assume a circular or near-circular reference orbit [1–4,6,9,10,13–16]
3. They assume a set of impulse times and do not solve for the optimal ones [15–21].
4. They minimize fuel use for each thrust axis independently [14,17].

Some of these issues may not be critical for certain specific mission profiles, but the goal of this paper is to design a general method for optimal maneuver targeting in circular or elliptic reference orbits, including the J_2 perturbation, which can be implemented on-board a spacecraft with limited computational power.

This goal is accomplished by using an approach similar to Lawden's primer vector theory [22], as in [1–8, 10, 11]. However, instead of solving the nonlinear equations directly, a suboptimal discrete-time formulation is iteratively refined using the necessary conditions of the continuous-time system to find the optimal impulse times. The discrete formulation is analytically solvable with the use of differential orbital elements as state variables. Similar discrete solvable formulations have been used by Breger and How [17], Roth [19],

978-1-4799-1622-1/14/$31.00

Saunders [16], Anderson and Schaub [20], and Gaias et al. [21], where the problem is broken up into many segments and the overall fuel cost is minimized, but these methods typically allow more impulses than necessary and do not find the true optimal times.

Of the previous work, only Gaias et al. [21] include differential drag in the analytical model, which is a primary consideration in low Earth orbit. However, it is extremely difficult to model this perturbation accurately for general spacecraft formations because of its dependence on the attitude and shape of both spacecraft and problems with modeling atmospheric density and surface interactions. In some cases, attempting to simulate drag effects with uncertain attitude and density knowledge can result in less accurate state propagation than if drag were not included in the force model at all [23]. Therefore, the present work does not address this perturbation, which implicitly invokes the assumption that either the ballistic coefficients of the spacecraft in the formation are very similar or the orbit altitude is high enough that differential drag effects are small.

The dynamic equations in this paper are developed in terms of mean orbital element differences rather than Cartesian coordinates. Differential orbital elements are a natural and convenient choice for designing general formations [24,25] as they provide several mathematical advantages over Cartesian coordinates for describing relative motion: they vary slowly, since they are constants of the unperturbed motion, and using mean elements allows for the explicit inclusion of secular J_2 effects. Furthermore, using a set of nearly-nonsingular elements makes the solution uniformly applicable to both circular and elliptic orbits. Although they provide indirect insight into the shape, size, and location of the relative orbit, they can be readily transformed into mission-useful quantities, such as size, orientation, etc., for visualization and analysis [26,27].

From the overall system design standpoint, the best approach to solving the problem is to use the most efficient mathematical form (differential mean orbital elements) to describe the dynamics but allow the formation designer to interact with more intuitive geometric quantities. The maneuver targeting problem is formulated as an optimal control problem in which the analytical solution to the unforced dynamics is given by the Gim-Alfriend state transition matrix (STM) [28] and the control influence is given by Gauss's Variational Equations (GVE) [29], re-formulated in terms of the nearly-nonsingular elements. Similar approaches have been used by previous authors to solve feedback control problems using classical mean orbital elements [17,30–32].

Several useful formation configurations have been developed using the well-known Hill-Clohessy-Wiltshire (HCW) [33, 34] equations, which describe the motion of a spacecraft formation in a circular, unperturbed reference orbit. These configurations are discussed at length by authors such as Fehse [35], Woffinden [36], Alfriend et al. [37], and others. In elliptic, unperturbed orbits, the dynamics are governed by the Tschauner-Hempel (TH) [38] or Lawden's [22] equations. A useful parametrization of the general solution to these equations was derived by Sengupta and Vadali [27] in terms of nearly-nonsingular elements. Using the conversions they provide, the method of this paper is employed by defining a desired formation in terms of HCW or TH parameters and then converting to differential elements for maneuver targeting.

Uncertainties in navigation and maneuvering systems, as well as unmodeled perturbations such as J_2 and atmospheric drag, will cause deviations from a desired HCW or TH trajectory over time. In particular, the greatest uncertainty will be encountered in the along-track direction, because that is the direction of orbital motion and any errors in relative orbital period will cause errors in the along-track drift rate. As noted by Carpenter and Alfriend [39], relative velocity errors are directly related to differential semimajor axis uncertainty (which determines the relative orbital period), which is usually the most important error in formation flying.

Along-track uncertainty and errors in along-track drift rate introduce substantial collision risk into any proximity operation. For example, the NASA DART mission ended unsuccessfully when the spacecraft collided with the MUBLCOM satellite during near-range acquisition maneuvers because of poor along-track navigation [40]. Recent authors such as Fehse [35], Naasz [41], D'Amico and Montenbruck [42], and Gaylor and Barbee [43] have discussed strategies for designing passively safe trajectories to mitigate collision risk without requiring frequent corrective thrusting. The same DART mission successfully used these types of passively safe trajectories during the long-range phases of the mission before transitioning to non-passively safe trajectories for near-range maneuvers. The DARPA Orbital Express mission avoided a collision during an abort maneuver and loss of navigation information thanks to the unintentional presence of out-of-plane motion which made its trajectory passively safe [44]. The European PRISMA and TanDEM-X/TerraSAR-X missions have both successfully used fuel efficient, passively safe trajectories for proximity operations as well.

The paper is laid out as follows. In Section 2, the formation dynamics are defined in terms of differential nearly-nonsingular mean orbital elements and the HCW and TH design parameters are summarized. The minimum-fuel maneuver targeting problem is defined in Section 3 and the necessary conditions for optimality are derived. Section 4 discusses a practical algorithm for on-board maneuver targeting, in which the discrete-time problem is iteratively solved while using the continuous-time necessary conditions to refine the thrust times until they converge to the optimal values. Finally, Section 5 provides simulation results for a variety of reconfiguration maneuvers and reference orbits. This includes simulations with and without navigation errors for the NASA CubeSat Proximity Operations Demonstration (CPOD) mission, as well as a comparison to the impulsive maneuver targeting method of Anderson and Schaub [20]. CPOD, sponsored by the NASA Office of the Chief Technologist, is to demonstrate formation flying and docking of a pair of 3U CubeSats using miniaturized navigation and propulsion. The algorithm defined in this paper is to form the basis of the CPOD guidance system for on-board maneuver planning.

2. FORMATION DYNAMICS

A general spacecraft formation consists of two or more space objects flying in close proximity to one another. The term "close" is defined such that the relative motion between the objects can be linearized about some reference orbit (this depends on the orbit of the formation and the required accuracy of the motion). Spacecraft in the formation can act either cooperatively or noncooperatively and the reference orbit need not correspond to an actual physical object. Without

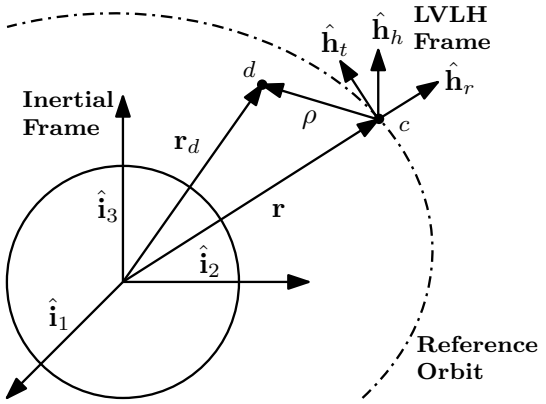

Figure 1. LVLH reference frame.

loss of generality, in this paper, the formation is assumed to consist of only two spacecraft. One spacecraft, which defines the reference orbit, is designated the "chief," and it is uncontrolled. The other spacecraft is designated the "deputy," and it is controlled by a 3-component thrust input.

The dynamics of relative motion are defined in terms of differential orbital elements, but formation configurations and visualizations are presented in Cartesian coordinates as well, using the local-vertical–local-horizontal (LVLH) reference frame. This frame, shown in Figure 1, is defined with $\hat{\mathbf{h}}_r$ in the radial direction, $\hat{\mathbf{h}}_h$ in the orbit normal direction, and $\hat{\mathbf{h}}_t$ completing the right-hand system. The mapping between differential orbital elements and LVLH coordinates can be found in a number of references, e.g. [26,28,45].

Formation Dynamics in Nearly-Nonsingular Mean Orbital Elements

The nearly-nonsingular mean orbital elements of the reference (chief) orbit are defined as

$$\boldsymbol{\alpha} = \begin{bmatrix} a & \lambda & i & q_1 & q_2 & \Omega \end{bmatrix}^T \tag{1}$$

where a is the semimajor axis, $\lambda = M + \omega$ is the mean argument of latitude, M is the mean anomaly, ω is the argument of perigee, i is the inclination, $q_1 = e\cos\omega$ and $q_2 = e\sin\omega$ are the orbital frame components of the eccentricity vector, e is the eccentricity, and Ω is the right ascension of the ascending node. This set of orbital elements is chosen instead of the classical orbital elements because it is not singular in the case of a circular orbit; however, it is still singular in an equatorial orbit.

The transformation from the osculating elements $\boldsymbol{\alpha}'$ to the mean elements is defined by

$$\boldsymbol{\alpha} = \mathbf{g}\left(\boldsymbol{\alpha}'\right) \tag{2}$$

The full transformation is given by Brouwer's analytical satellite theory [46], and a first-order truncation is given by Schaub and Junkins [47]. Including the effects of J_2, the mean elements evolve according to

$$\dot{\boldsymbol{\alpha}} = \mathbf{f}\left(\boldsymbol{\alpha}\right) + \mathbf{g}\left(\mathbf{B}\left(\boldsymbol{\alpha}'\right)\mathbf{u}\right) \tag{3}$$

where $\mathbf{u}$ is a thrust input defined in the LVLH frame,

$$\mathbf{u} = \begin{bmatrix} u_r & u_t & u_h \end{bmatrix}^T \tag{4}$$

whose effect on the osculating orbital elements is given by a modified form (to use the nearly-nonsingular elements) of Gauss's Variational Equations (GVE) $\mathbf{B}\left(\boldsymbol{\alpha}'\right)$, given in Appendix A. Since GVE give the effect of accelerations on the osculating elements, the osculating–mean transformation must then be applied to determine changes in the mean elements. However, the sensitivities of mean element changes with respect to osculating element changes are of at most $\mathcal{O}\left(J_2\right)$; therefore, for small accelerations it is reasonable to approximate Eq. (3) by [30,31]

$$\dot{\boldsymbol{\alpha}} \approx \mathbf{f}\left(\boldsymbol{\alpha}\right) + \mathbf{B}\left(\boldsymbol{\alpha}\right)\mathbf{u} \tag{5}$$

The unforced dynamics are given by a modified form of Lagrange's Planetary Equations (LPE) for J_2 [29],

$$\mathbf{f}\left(\boldsymbol{\alpha}\right) = \begin{bmatrix} 0 \\ n + \frac{3}{4}J_2\left(\frac{R_e}{p}\right)^2 n\left[\eta\left(3\cos^2 i - 1\right) + \left(5\cos^2 i - 1\right)\right] \\ 0 \\ -\frac{3}{4}J_2\left(\frac{R_e}{p}\right)^2 n\left(3\cos^2 i - 1\right) q_2 \\ \frac{3}{4}J_2\left(\frac{R_e}{p}\right)^2 n\left(3\cos^2 i - 1\right) q_1 \\ -\frac{3}{2}J_2\left(\frac{R_e}{p}\right)^2 n\cos i \end{bmatrix} \tag{6}$$

where J_2 is the coefficient of the second zonal harmonic, R_e is the mean equatorial radius of the Earth, p is the semilatus rectum, n is the mean motion, and $\eta = \sqrt{1-e^2}$.

The motion of the deputy about the reference orbit is described by a set of differential mean orbital elements, which are related to the deputy's mean elements by

$$\delta\boldsymbol{\alpha} = \boldsymbol{\alpha}_d - \boldsymbol{\alpha} \tag{7}$$

Assuming the differences between the deputy's mean elements and the reference elements are small, the dynamics of the differential mean elements are found by linearizing Eq. (5) about the reference orbit:

$$\delta\dot{\boldsymbol{\alpha}} = \mathbf{A}\delta\boldsymbol{\alpha} + \mathbf{B}\mathbf{u} \tag{8}$$

where $\mathbf{B}$ is GVE evaluated on the reference orbit and

$$\mathbf{A} = \left.\frac{\partial \mathbf{f}}{\partial \boldsymbol{\alpha}}\right|_{\boldsymbol{\alpha}} \tag{9}$$

is the Jacobian of LPE evaluated on the reference orbit. The definition of $\mathbf{A}$ is found in Appendix B.

State Transition Matrix for the Differential Elements—The general solution to Eq. (8) is given by

$$\delta\boldsymbol{\alpha}\left(t\right) = \boldsymbol{\Phi}\left(t, t_0\right)\delta\boldsymbol{\alpha}\left(t_0\right) + \int_{t_0}^{t} \boldsymbol{\Phi}\left(t,\tau\right)\mathbf{B}\left(\tau\right)\mathbf{u}\left(\tau\right)\, d\tau \tag{10}$$

where $\boldsymbol{\Phi}\left(t_2, t_1\right)$ is the state transition matrix (STM) of $\mathbf{A}$ from t_1 to t_2. The STM for the differential nearly-nonsingular mean orbital elements is derived by Gim and Alfriend [28]. The STM found in that paper requires a small modification due to the fact that it uses the true argument of latitude $\theta = f + \omega$ instead of the mean argument of latitude λ. For formations in near-circular reference orbits, significant computation effort is saved by using the small-eccentricity version of the STM given by Alfriend and Yan [48].

Characterization of Relative Motion in Circular or Elliptic Orbits

The motion of the deputy relative to the chief in the LVLH frame in a general unperturbed elliptic orbit is governed by the Tschauner-Hempel (TH) [38] or Lawden's [22] equations. Note that in the following development, the relative motion is not restricted to periodic solutions, which allows for the definition of more generic rendezvous trajectories in addition to standard proximity operations. A useful parametrization of the general solution to these equations is derived by Sengupta and Vadali [27] in terms of nearly-nonsingular elements:

$$x(\theta) = \rho_1 \sin(\theta + \tilde{\alpha}_0) - \frac{2v_d}{3n\eta^2}\left[\frac{r}{p} - \frac{3(q_1 \sin\theta - q_2 \cos\theta)}{2\eta^3} K(\theta)\right] \tag{11}$$

$$y(\theta) = \frac{\rho_1 r}{p}(2 + q_1 \cos\theta + q_2 \sin\theta)\cos(\theta + \tilde{\alpha}_0) + \frac{\rho_2 r}{p} + \frac{v_d p}{rn\eta^5} K(\theta) \tag{12}$$

$$z(\theta) = \frac{\rho_3 r}{p} \sin\left(\theta + \tilde{\beta}_0\right) \tag{13}$$

where $K(\theta)$ is an implicit function of θ,

$$K(\theta) = \lambda - \lambda_0 = n(t - t_0) \tag{14}$$

x, y, z are the components of the relative position $\boldsymbol{\rho}$ in the LVLH frame, and ρ_1, ρ_2, ρ_3, v_d, $\tilde{\alpha}_0$, and $\tilde{\beta}_0$ are the parameters that define the relative trajectory. ρ_1 and ρ_3 relate to the amplitude of the in-plane and out-of-plane motion, $\tilde{\alpha}_0$ and $\tilde{\beta}_0$ are the initial phase angles, ρ_2 determines how far offset the motion is in the along-track direction, and v_d is the along-track drift rate. The presence of the time-varying orbit radius r in many of these terms means that the motion does not correspond to a simple oscillator in an elliptic orbit.

If the reference orbit is circular, Eqs. (11)–(13) simplify to the well-known Hill-Clohessy-Wiltshire (HCW) [33, 34] equations,

$$x(t) = \rho \sin(nt + \alpha_0) - \frac{2v_d}{3n} \tag{15}$$

$$y(t) = 2\rho \cos(nt + \alpha_0) + d + v_d(t - t_0) \tag{16}$$

$$z(t) = \rho_z \sin(nt + \beta_0) \tag{17}$$

In this case, ρ and ρ_z correspond precisely to the amplitude of the in-plane and out-of-plane motion, the in-plane motion is the superposition of a 2-1 ellipse and a linear drift in the along-track direction at a rate of v_d, and d is the along-track offset of the initial in-plane ellipse. Any along-track drift also induces a small constant radial offset. Several useful trajectories for proximity operations and rendezvous are specified by choosing different values of these parameters. These are discussed at length by authors such as Woffinden [36], Alfriend et al. [37], and others.

Several authors [26, 27, 45, 49–51] have analyzed the effects of eccentricity on the HCW trajectories. The most significant effects of eccentricity are the distortion of the harmonic motion, the introduction of an along-track bias in the in-plane motion, a shift in phase for both α_0 and β_0, and oscillation of the along-track offset d. Sengupta and Vadali [27] suggest a number of possible corrections to make the elliptical motion more closely approximate a desired HCW trajectory, although it will never be possible to match it exactly. For example, setting

$$\rho_{2a} = \frac{2\eta^2 d}{3 - \eta^2} \tag{18}$$

in a leader-follower configuration modifies the along-track offset so that the time-averaged deputy-chief separation is d. Similarly, setting

$$\rho_{2b} = \rho(q_1 \cos\alpha_0 - q_2 \sin\alpha_0) \tag{19}$$

in an in-plane ellipse with $d = 0$ corrects the along-track bias so that $y(-\alpha_0) = 2\rho$ and $y(\pi - \alpha_0) = -2\rho$ (this is just one possible bias correction). For an in-plane ellipse with non-zero d, use $\rho_2 = \rho_{2a} + \rho_{2b}$. Both of these equations reduce to the HCW parameters in circular orbits. Additional corrections are possible for the other parameters as well, but this paper only employs the two, so that $\rho_1 = \rho$, $\rho_3 = \rho_z$, $\tilde{\alpha}_0 = \alpha_0$, and $\tilde{\beta}_0 = \beta_0$.

Initial Differential Elements for General Formations

In order for the trajectory designer to make use of the dynamic formulation in terms of differential orbital elements, relationships are required to convert the TH (or HCW) parameters into nearly-nonsingular element differences. Sengupta and Vadali [27] provide the required equations, which are summarized here for reference:

$$\delta a = \frac{-2\eta v_d}{3n} \tag{20}$$

$$\delta\lambda = \frac{\rho_2}{p} - \delta\Omega\cos i - \frac{1 + \eta + \eta^2}{1 + \eta}\frac{\rho_1}{p}(q_1 \cos\tilde{\alpha}_0 - q_2 \sin\tilde{\alpha}_0) \tag{21}$$

$$\delta i = \frac{\rho_3}{p}\cos\tilde{\beta}_0 \tag{22}$$

$$\delta q_1 = -\left(1 - q_1^2\right)\frac{\rho_1}{p}\sin\tilde{\alpha}_0 + q_1 q_2 \frac{\rho_1}{p}\cos\tilde{\alpha}_0 - q_2\left(\frac{\rho_2}{p} - \delta\Omega\cos i\right) \tag{23}$$

$$\delta q_2 = -\left(1 - q_2^2\right)\frac{\rho_1}{p}\cos\tilde{\alpha}_0 + q_1 q_2 \frac{\rho_1}{p}\sin\tilde{\alpha}_0 + q_1\left(\frac{\rho_2}{p} - \delta\Omega\cos i\right) \tag{24}$$

$$\delta\Omega = \frac{-\rho_3}{p}\frac{\sin\tilde{\beta}_0}{\sin i} \tag{25}$$

J_2 Perturbation Effects—A number of authors [26,45,52–54] have also investigated the effects of the J_2 perturbation on the HCW and TH trajectories. It is possible to impose conditions on the initial differential mean elements to design J_2-invariant relative orbits (in the mean sense) for formation flying, as discussed by Schaub and Alfriend [53]. However, this requires imposing three constraints, leaving only three degrees of freedom for trajectory design. Instead, it is common to enforce only one constraint on the differential semimajor axis, which mitigates along-track drift due to J_2 and keeps the long-term motion bounded. Note that the magnitude of this constraint is approximately proportional to the eccentricity plus the magnitude of the out-of-plane motion, so the correction is negligible for near-circular orbits with very little out-of-plane motion.

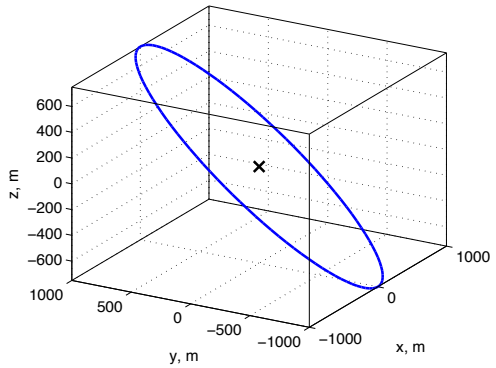

Figure 2. Safety ellipse example.

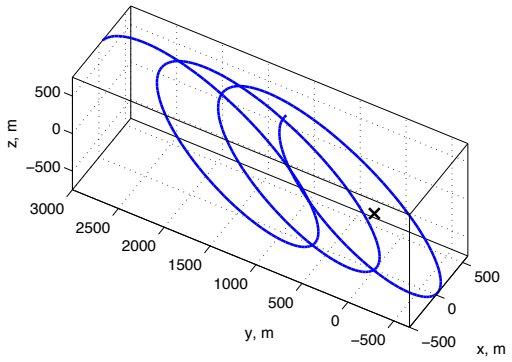

Figure 3. Walking safety ellipse example.

Passively Safe Trajectories

Passively safe trajectories are designed by using a combination of in-plane and out-of-plane harmonic motion with initial phase angles selected so that the trajectory never crosses the along-track axis. In this way, if the deputy is unintentionally drifting towards the chief in the along-track direction, they cannot collide since the deputy never actually crosses the along-track axis. Maximum "safety" is achieved when the phase angles are chosen such that $\beta_0 = \alpha_0 \pm \frac{\pi}{2}$ since this maximizes the distance between the deputy and the along-track axis when either $x = 0$ or $z = 0$. This paper uses the nomenclature of Fehse [35], Naasz [41], and Gaylor and Barbee [43], which refers to this type of trajectory as a "safety ellipse," and an example is shown in Figure 2. The same strategy is used to achieve passively safe rendezvous by introducing a non-zero along-track drift rate (which introduces a corresponding radial offset) and initial along-track offset along with the same ellipse definition. This trajectory is referred to as a "walking safety ellipse," and an example is shown in Figure 3.

3. Fuel-Optimal Targeting of n-Impulse Maneuvers

The main problem addressed in this paper is that of finding optimal minimum-fuel maneuvers, made up of n impulsive thrusts, for formation reconfiguration. In this paper, unlike some other formulations, the minimum-fuel problem is stated in terms of the 2-norm of the thrust input instead of 1-norm. In general, even if multiple thrusters are available, it saves fuel to align the net thrust direction with one of the thrusters (or pair of co-aligned thrusters) when thrust is required in more than one LVLH direction, due to the triangle inequality. The fuel savings are greater for larger maneuvers, as the extra fuel cost is proportional to the total cost. That is, for smaller maneuvers, it might make more sense, operationally, to spend the small amount of extra fuel to use multiple thrusters to achieve a maneuver and not disrupt the attitude of the spacecraft.

In this section, the minimum-fuel n-impulse maneuver targeting problem is stated in both continuous- and discrete-time forms and the necessary conditions for optimality are derived. Neither of these formulations adequately solves the problem on its own, but recognizing the duality of the continuous and discrete formulations under certain conditions allows a convenient solution to be found. In the section that follows, a practical algorithm for on-board maneuver targeting is described which uses an iterative refinement of the discrete-time form of the problem to solve for the optimal thrust times and impulse magnitudes.

Continuous-Time Optimal Control Problem

First, the minimum-fuel problem is defined in terms of the continuous-time dynamics. The analysis is similar to a formation flying application of Lawden's primer vector [22] theory, which is described in detail by McAdoo et al. [55] and Jezewski [56]. A number of previous authors have used primer vector theory to address the formation reconfiguration problem in terms of Cartesian states [1–8, 10, 11]. The difference in this formulation is that the primer vector now depends on all six orbit element costates through GVE, which are time-varying, instead of only on the three-component velocity costate as in the Cartesian case.

The fuel cost for an n-impulse maneuver is defined as

$$J = \int_0^{t_n} \gamma(t)\ dt \tag{26}$$

where $\gamma(t)$ is the impulse magnitude at time t, such that

$$\gamma(t) = \gamma_1 \delta(t - t_1) + \gamma_2 \delta(t - t_2) + \ldots + \gamma_n \delta(t - t_n) \tag{27}$$

and the thrust is defined by

$$\mathbf{u} = \gamma \hat{\mathbf{u}} \tag{28}$$

$\delta(t - t_i)$ is the Dirac delta function and all $\gamma_i > 0$. Note that the final impulse is constrained to occur at the final time, which is free. According to the sifting property of delta function, this cost is exactly the sum of the impulse magnitudes:

$$J = \sum_{i=1}^{n} \gamma_i \tag{29}$$

which is the total ΔV of the maneuver. The control goal is to determine the optimal γ_i, t_i, and $\hat{\mathbf{u}}$ to take the system from a fixed initial state $\delta\mathbf{oe}_0$ to a desired final state $\delta\mathbf{oe}_n = \delta\mathbf{oe}_f$ (fixed final state).

Necessary Conditions for Optimality—Incorporating the system dynamics defined in Eq. (8), the Hamiltonian can be written,

$$H = \gamma + \boldsymbol{\lambda}^T (\mathbf{A}\delta\mathbf{oe} + \gamma \mathbf{B}\hat{\mathbf{u}}) \tag{30}$$

On an optimal trajectory, the costate equation is

$$\dot{\boldsymbol{\lambda}} = -H_{\delta\mathbf{oe}} = -\mathbf{A}^T\boldsymbol{\lambda} \tag{31}$$

and both the costate and its derivative must be continuous. The solution to the costate equation is given by

$$\boldsymbol{\lambda}(t) = \boldsymbol{\Phi}^T(t_0, t)\,\boldsymbol{\lambda}(t_0) \tag{32}$$

(See proof in Appendix C.) Since the control direction $\hat{\mathbf{u}}$ appears linearly in H, the optimal control cannot be determined directly from the stationary condition. Applying Pontryagin's minimum principle, the control direction which minimizes the Hamiltonian is

$$\hat{\mathbf{u}} = -\mathbf{B}^T\boldsymbol{\lambda} = -\mathbf{p} \tag{33}$$

where $\mathbf{p}$ is defined as the primer vector, which a formation flying analogue to Lawden's primer vector [22]. As mentioned above, the difference between this formulation and previous primer vector-based formation flying analyses is that $\mathbf{p}$ now depends on all six orbit element costates through GVE, the time-varying $\mathbf{B}$ matrix, instead of only on the three-component velocity costate.

Applying the necessary condition for the control direction, the Hamiltonian then becomes

$$H = \left(1 - \mathbf{p}^T\mathbf{p}\right)\gamma + \boldsymbol{\lambda}^T\mathbf{A}\delta\mathbf{oe} \tag{34}$$

Since H must be continuous along an optimal trajectory, the coefficient of γ must be zero when each impulse is applied:

$$\|\mathbf{p}\| = p = 1 \quad , \quad \forall\, t = t_i \tag{35}$$

At other times, for the trajectory to be optimal, $p < 1$ or else Pontryagin's minimum principle would imply that the trajectory is non-optimal since some additional non-zero γ exists which would decrease the Hamiltonian. In addition, $\boldsymbol{\lambda}$ and therefore $\mathbf{p}$ must be continuous across the impulses. Since $p < 1$ before and after each impulse, then $\dot{p} = 0$ at those points (this includes the final impulse since t_n is free and must also obey Pontryagin's minimum principle). That is,

$$\dot{\mathbf{p}}^T\mathbf{p} = 0 \quad , \quad \forall\, t = t_i \tag{36}$$

assuming without loss of generality that $t_1 \neq 0$. If $t_1 = 0$ and this condition is not satisfied, then there exists a $t_1 < 0$ which will have a lower cost.

Continuity of the Hamiltonian also requires that $H^+ = H^-$ for each impulse,

$$\begin{aligned} 0 = H^+ - H^- &= \boldsymbol{\lambda}^T\mathbf{A}\left(\delta\mathbf{oe}^+ - \delta\mathbf{oe}^-\right) \\ &= \dot{\boldsymbol{\lambda}}^T\mathbf{B}\mathbf{B}^T\boldsymbol{\lambda}\gamma_i \end{aligned} \tag{37}$$

Together, Eqs. (36) and (37) then imply the two conditions

$$\left(\mathbf{B}^T\dot{\boldsymbol{\lambda}}\right)^T\left(\mathbf{B}^T\boldsymbol{\lambda}\right) = 0 \quad , \quad \forall\, t = t_i \tag{38}$$

$$\left(\dot{\mathbf{B}}^T\boldsymbol{\lambda}\right)^T\left(\mathbf{B}^T\boldsymbol{\lambda}\right) = 0 \quad , \quad \forall\, t = t_i \tag{39}$$

In Lawden's primer vector theory, the $\mathbf{B}$ matrix is constant and these constraints reduce to the familiar $\dot{p} = 0$ condition. For the final time free problem, the last condition is given by

$$0 = H(t_n) = \boldsymbol{\lambda}_n^T\mathbf{A}(t_n)\,\delta\mathbf{oe}_f = -\dot{\boldsymbol{\lambda}}_n^T\delta\mathbf{oe}_f \tag{40}$$

where $\boldsymbol{\lambda}_n = \boldsymbol{\lambda}(t_n)$. This implies that the optimal final time occurs when the derivative of the costate is perpendicular to the desired state (or, equivalently, when the costate is perpendicular to the derivative of the desired state).

Computation Difficulties—The continuous-time optimal control problem is challenging to solve because of the nonlinearity of the problem. When the necessary conditions are applied, the result is a set of coupled nonlinear differential equations. Even if the state and costate dynamics are enforced explicitly, these still result in a set of coupled nonlinear algebraic equations. Techniques exist in the literature to solve this problem using the traditional primer vector formulation, e.g. [1, 55–58], by beginning with two impulses and adding additional ones until the optimal maneuver is obtained. However, these techniques do not apply directly to the present problem since the primer vector now depends on all six elements of the costate through the time-varying GVE and it is more challenging to obtain a compatible initial estimate for the costate, especially when adding an additional impulse. Furthermore, all of these techniques require a multi-dimensional nonlinear solver, which will be subject to convergence and multiple solution issues, and it simply may not be practical to implement such an algorithm on-board a small spacecraft.

Discrete-Time Optimal Control Problem

Instead of expressing the minimum-fuel problem in terms of the continuous dynamics, it can be stated as a discrete-time optimal problem:

$$J_d = \frac{1}{2}\sum_{k=1}^{N}\mathbf{u}_k^T\mathbf{u}_k \tag{41}$$

subject to the discrete dynamics

$$\delta\mathbf{oe}_{k+1} = \boldsymbol{\Phi}_k\delta\mathbf{oe}_k + \boldsymbol{\Gamma}_k\mathbf{u}_k \tag{42}$$

where

$$\boldsymbol{\Phi}_k = \boldsymbol{\Phi}(t_{k+1}, t_k) \tag{43}$$

$$\boldsymbol{\Gamma}_k = \boldsymbol{\Phi}(t_{k+1}, t_k)\,\mathbf{B}(t_k) \tag{44}$$

for impulsive control. $\boldsymbol{\Phi}(t_{k+1}, t_k)$ is the STM defined in Eq. (10). The cost in Eq. (41) is the sum of the squares of the impulse magnitudes at the N discretization points, which is slightly different than the cost in Eq. (29). However, if $N = n$ and the t_k were placed at the optimal times t_i, then minimizing Eq. (41) would be equivalent to minimizing Eq. (29).

A number of previous authors have also used discrete-time formulations such as this to address the reconfiguration problem, e.g. [14, 16–21]. Most of these arrive at different solutions since they use different cost functions, make simplifying assumptions about the reference orbit, or use alternate methods to derive the thrust input or optimality conditions. However, some of them do arrive at the same solution under certain conditions and choices of thrust times. The main difference in this paper compared to previous methods is that the discrete formulation is solved iteratively so that the thrust times converge to the optimal times of the continuous formulation.

Necessary Conditions for Optimality—The Hamiltonian for the discrete-time problem is

$$H_d = \frac{1}{2}\mathbf{u}_k^T\mathbf{u}_k + \boldsymbol{\Lambda}_{k+1}^T\left(\boldsymbol{\Phi}_k\delta\mathbf{oe}_k + \boldsymbol{\Gamma}_k\mathbf{u}_k\right) \tag{45}$$

For an optimal control sequence, the costate equation is

$$\boldsymbol{\Lambda}_k = H^d_{\delta\mathbf{oe}_k} = \boldsymbol{\Phi}_k^T\boldsymbol{\Lambda}_{k+1} \tag{46}$$

The optimal control is given by the stationary condition,

$$0 = H^d_{\mathbf{u}_k} = \mathbf{u}_k + \mathbf{\Gamma}^T_k \mathbf{\Lambda}_{k+1} \tag{47}$$

$$\mathbf{u}_k = -\mathbf{\Gamma}^T_k \mathbf{\Lambda}_{k+1} \tag{48}$$

Since $\mathbf{\Phi}_k$ is invertible, the combined state-costate system can be written as

$$\begin{bmatrix} \delta\boldsymbol{\alpha}_k \\ \mathbf{\Lambda}_k \end{bmatrix} = \begin{bmatrix} \mathbf{\Phi}_k^{-1} & \mathbf{B}_k\mathbf{B}_k^T\mathbf{\Phi}_k^T \\ \mathbf{0} & \mathbf{\Phi}_k^T \end{bmatrix} \begin{bmatrix} \delta\boldsymbol{\alpha}_{k+1} \\ \mathbf{\Lambda}_{k+1} \end{bmatrix}$$
$$\mathbf{z}_k = \mathbf{\Psi}_k \mathbf{z}_{k+1} \tag{49}$$

where $\mathbf{B}_k = \mathbf{B}(t_k)$. Proceeding backwards in time, the solution to Eq. (49) is

$$\mathbf{z}_1 = \mathbf{\Xi}_{1,N+1}\mathbf{z}_{N+1} \tag{50}$$

defining

$$\mathbf{\Xi}_{1,N+1} = \begin{bmatrix} \boldsymbol{\xi}_{11} & \boldsymbol{\xi}_{12} \\ \boldsymbol{\xi}_{21} & \boldsymbol{\xi}_{22} \end{bmatrix} = \prod_{k=1}^{N} \mathbf{\Psi}_k \tag{51}$$

Expanding the first component of $\mathbf{z}_1$ gives

$$\delta\boldsymbol{\alpha}_1 = \mathbf{\Phi}(t_1, 0)\,\delta\boldsymbol{\alpha}_0 = \boldsymbol{\xi}_{11}\delta\boldsymbol{\alpha}_f + \boldsymbol{\xi}_{12}\mathbf{\Lambda}_{N+1} \tag{52}$$

where $\delta\boldsymbol{\alpha}_1 = \delta\boldsymbol{\alpha}(t_1)$, since the first impulse does not necessarily occur at $t = 0$. Note that the desired state in the discrete formulation is specified at t_{N+1}. Assuming $\boldsymbol{\xi}_{12}$ is invertible, $\mathbf{\Lambda}_{N+1}$ can then be written in terms of the initial and desired final state:

$$\mathbf{\Lambda}_{N+1} = \boldsymbol{\xi}_{12}^{-1}\left[\mathbf{\Phi}(t_1, 0)\,\delta\boldsymbol{\alpha}_0 - \boldsymbol{\xi}_{11}\delta\boldsymbol{\alpha}_f\right] \tag{53}$$

Note that because the unperturbed STM contains orbit-periodic terms with in-plane and out-of-plane motion decoupled, there will be cases when $\boldsymbol{\xi}_{12}$ is singular for certain thrust times if only two impulses are used (or nearly singular for perturbed orbits). In these cases, not all components of the final costate are uniquely determined by Eq. (52), and a minimum-norm solution for $\mathbf{\Lambda}_{N+1}$ will give the optimal control. However, if the thrust times are nowhere near the optimal thrust times, the solution may not be practically feasible, i.e. it could result in unrealistically large impulses.

4. Design of a Practical Algorithm for On-Board Maneuver Targeting

The solution to the minimum-fuel n-impulse maneuver problem is given by the continuous-time optimal control formulation, rather than the discrete formulation, in general. This is because the thrust times in the discrete formulation are specified *a priori* by the choice of discretization times. If a fine discretization time spacing is used, the optimal thrust times may be found but more thrusts will occur than necessary since the control is determined by the costate which evolves according to the continuous dynamics and cannot simply become zero for several time steps when the optimal trajectory should have a coast arc.

However, the discrete-time optimal control problem is relatively simple to solve: it involves a number of large matrix multiplications and the inversion of a 6×6 matrix. The key to designing a practical algorithm for on-board maneuver targeting is recognizing the link between the discrete and continuous formulations. Since the state transition matrix solution to the dynamics is known explicitly and the control is impulsive, there is no need for the discretization times to be close together or equally spaced, and the final time t_{N+1} can be arbitrarily chosen to be the same as the final control time t_N. As mentioned previously, if the t_k are placed exactly at the optimal times t_i, then the discrete optimal control sequence is also optimal in the continuous formulation.

In that case, the control at each t_i is the same in both the continuous and discrete formulations:

$$\mathbf{u}_i = -\mathbf{B}_i^T\mathbf{\Phi}^T(t_n, t_i)\,\mathbf{\Lambda}_n = -\gamma_i\mathbf{B}_i^T\mathbf{\Phi}^T(t_n, t_i)\,\boldsymbol{\lambda}_n \tag{54}$$

since $\mathbf{\Lambda}_{N+1} = \mathbf{\Lambda}_N$, $N = n$, and where $\mathbf{B}_i = \mathbf{B}(t_i)$. $\boldsymbol{\lambda}_n$ can then be found by solving the linear system

$$\begin{bmatrix} -\gamma_1\mathbf{B}_1^T\mathbf{\Phi}^T(t_n, t_1) \\ -\gamma_2\mathbf{B}_2^T\mathbf{\Phi}^T(t_n, t_2) \\ \vdots \\ -\gamma_n\mathbf{B}_n^T \end{bmatrix} \boldsymbol{\lambda}_n = \begin{bmatrix} \mathbf{u}_1 \\ \mathbf{u}_2 \\ \vdots \\ \mathbf{u}_n \end{bmatrix} \tag{55}$$

This system is guaranteed to have an exact solution since all of the necessary conditions for optimality of the continuous formulation are satisfied under these assumptions.

If the t_k are not placed at the optimal times, then the discrete optimal control sequence will not be optimal in the continuous formulation, but it will still represent a feasible solution since it satisfies the final state constraint. In this case, Eq. (55) may not have an exact solution. However, if the t_k are close to the optimal times, then a least squares solution of Eq. (55) will give an approximation of the final costate, but it will not satisfy the necessary conditions for optimality. By examining the resulting primer vector magnitude history it is possible to use the analysis of Lawden [22], Lion and Handelsman [57], and Jezewksi and Rozendaal [58] to improve the trajectory. That analysis identifies two important criteria for improving a suboptimal trajectory:

1. Moving an impulse: if $\dot{p} \neq 0$ at any impulse, move the impulse time slightly in the direction of increasing p.
2. Adding an impulse: if $p > 1$ somewhere other than near an impulse, add another impulse at the time of maximum p.

However, those methods always begin with two impulses and add more as required for optimality, whereas this algorithm may begin with a suboptimal solution with too many impulses. Therefore, one additional criterion is defined for removing an impulse:

3. Removing an impulse: if $p < 1$ and $\dot{p} = 0$ at any impulse, remove the impulse.

The improved trajectory is determined by re-solving the discrete optimal control problem with the new impulse times t_k. In any case, the maximum number of impulses required for the optimal maneuver is six. This is determined from a result by Neustadt [59] and Potter and Stern [60] which states that for a linear system the maximum number of impulses necessary to realize an optimal transfer is the number of constraints on the state variables at the final time. Practically speaking, four impulses is usually sufficient for an in-plane maneuver, since the out-of-plane coupling is of $\mathcal{O}(J_2)$.

To obtain an initial estimate for the optimal thrust times, solve the discrete optimal control problem using a large number

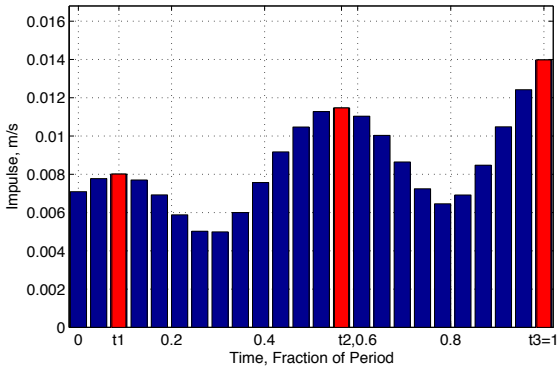

Figure 4. Impulse magnitudes for 24-impulse maneuver, identifying candidate optimal impulse times.

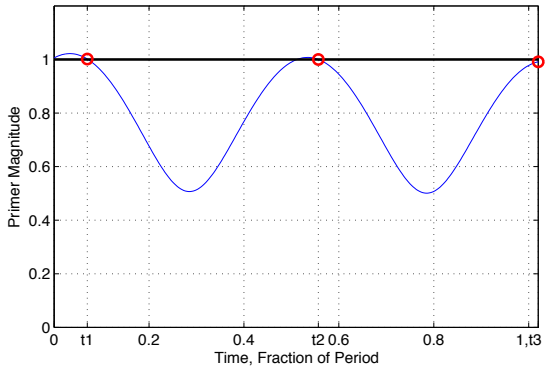

Figure 6. Primer history for partly refined suboptimal 3-impulse maneuver.

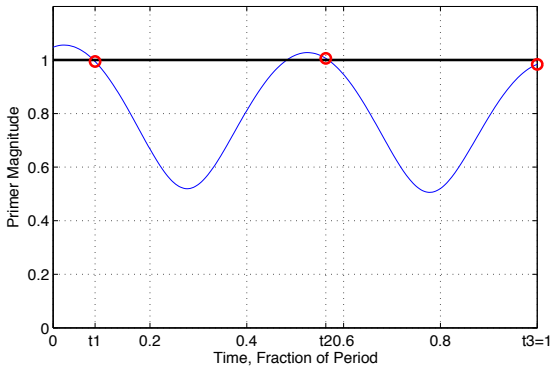

Figure 5. Primer history for suboptimal 3-impulse maneuver using candidate optimal impulse times.

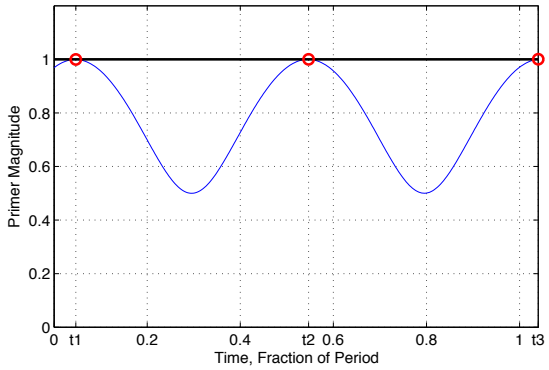

Figure 7. Primer history for optimal 3-impulse maneuver.

of impulses, e.g. 12 or more. Note that the total maneuver duration used to generate the initial estimate is implicitly assumed to be the approximate maximum maneuver duration. The final solution obtained using this algorithm is a local optimum in the vicinity of this maneuver duration. That is, the final optimal maneuver may have a duration of less than or slightly greater than the original duration, but the algorithm will not find optimal maneuvers with durations multiple orbits greater than the initial estimate. For maneuvers without large along-track, i.e. anomaly, changes, 1–2 orbits is typically a sufficient duration. For pure along-track maneuvers, or maneuvers with large along-track changes, the optimal maneuver duration is actually infinite, so the maximum maneuver duration must instead be dictated by mission constraints—this algorithm then finds the closest locally optimal maneuver (see Section 5 for an example of a pure along-track maneuver).

Table 1. Total Fuel Cost for Maneuver

Maneuver	ΔV, m/s
2-impulse from [14]	0.3316
24-impulse	0.2050
Suboptimal 3-impulse	0.1694
Partly Refined 3-impulse	0.1669
Optimal 3-impulse	0.1658

After solving the discrete optimal control problem using a large number of impulses, examine the resulting impulse magnitude history and select the times of any local maxima as estimates for the optimal thrust times. This technique quickly identifies the likely optimal number of impulses, and it eventually converges to the continuous-time optimal solution. In practice, though, it may not be necessary to determine the optimal thrust times exactly. Thrust magnitude and alignment errors, minimum impulse limits, finite thrust approximations, on-board navigation and timing inaccuracies, and other error sources mean that there is a point at which the improvement in going from a suboptimal to an optimal trajectory is below the threshold realizable by the actual system. Therefore, it is possible to define an algorithm which incrementally improves a suboptimal trajectory until the improvement in fuel cost (or the changes in thrust application times) is below some threshold, at which point the problem is considered "solved." The solution is the optimal number of impulses n, their application times $\{t_1, t_2, \ldots, t_n\}$, and the final costate $\mathbf{\Lambda}_{N+1}$, which yields the optimal impulses through Eqs. (46) and (48).

For example, the impulse magnitude history for a 24-impulse in-plane reconfiguration is shown in Figure 4 (for a circular, unperturbed reference orbit). The optimal number of impulses appears to be three and the candidate optimal thrust times (t_1, t_2, and t_3) are identified at the peak impulse locations, shown in red in the figure. After re-solving the discrete problem using the new impulse times, the least squares solution of Eq. (55) results in the primer magnitude history shown in Figure 5, with the impulse locations indicated as red

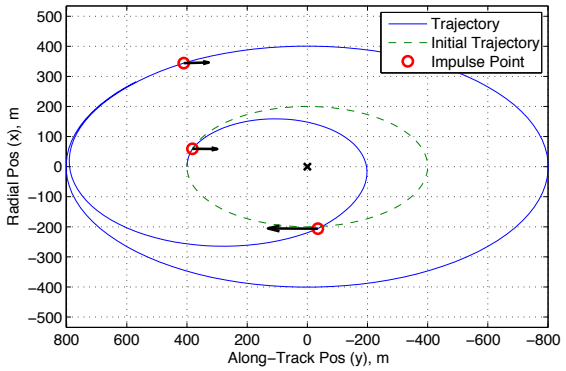

Figure 8. Optimal planar 3-impulse maneuver, $e = 0$.

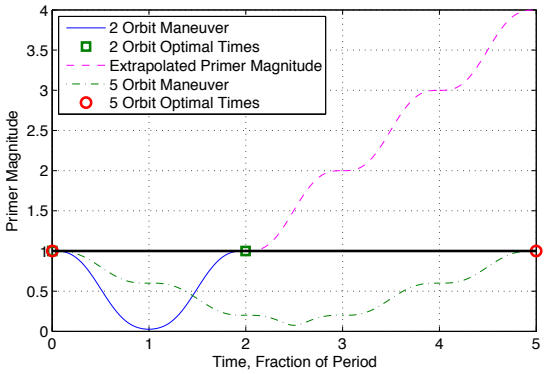

Figure 9. Primer history for pure along-track maneuver.

circles (note that the primer magnitude at each impulse is not exactly equal to one, as expected). The criteria above indicate that the trajectory can be improved by slightly decreasing t_1 and t_2 and increasing t_3, which results in the refined primer magnitude history shown in Figure 6 once the discrete problem has been re-solved. Continuing to refine the thrust times in this fashion eventually results in the optimal primer magnitude history of Figure 7, which corresponds to the trajectory shown in Figure 8. The total ΔV fuel cost required for each of these iterations is listed in Table 1 along with the corresponding 2-impulse solution from Vaddi et al. [14].

5. Simulation Results

Next, the ability of the algorithm of Section 4 to target general reconfiguration maneuvers is demonstrated. Several example maneuvers are considered for circular and elliptic orbits, with and without J_2. Maneuvers planned with J_2 included in the dynamics are simulated with J_2–J_6. Maneuvers are also simulated for the reference orbit of the CPOD mission, showing the effects of typical navigation and thrust errors.

Circular Orbit

Circular orbits are an important case to consider for any formation flying algorithm because of the breadth of interest in the aerospace community for applications and theory in such orbits. Classical orbital element methods fall short in this respect because the reference orbit parameters become singular for $e = 0$, reducing to a set of 5 independent quantities, while the deputy still requires 6 quantities to describe its relative orbit. Since this paper uses the nearly-nonsingular elements, the algorithm described here is uniformly applicable to both circular and elliptic orbits without modification (except when $i = 0$). The first circular orbit example is described in the previous section, a reconfiguration from a $\rho = 200$ m, $\alpha_0 = 0$ in-plane ellipse to a $\rho = 400$ m, $\alpha_0 = \frac{\pi}{4}$ in-plane ellipse, simulated without perturbations.

Pure Along-Track Maneuver—Another important case to consider is a reconfiguration between two leader-follower formations, a pure along-track or anomaly change, also known as a "V-Bar maneuver." This maneuver is challenging to design because the optimal maneuver times are spaced infinitely far apart. This is because the optimal maneuver uses the natural anomaly drift of the dynamics to create the desired anomaly change by introducing a small non-zero semimajor axis difference. For example, considering only tangential thrust, the optimal 2-impulse maneuver is

$$\Delta V_1 = -\frac{1}{3}\frac{\Delta d}{N_{\text{orb}} T} = -\Delta V_2 \tag{56}$$

where ΔV_1 and ΔV_2 are the two tangential impulses, spaced an integer number N_{orb} of orbits periods T apart, and Δd is the desired change in along-track position. Since the total fuel cost is inversely proportional to the duration, the optimal maneuver has an infinitesimal fuel cost and infinite duration.

However, this algorithm still finds the suboptimal maneuver for a given maneuver duration. The optimal primer histories for the two orbit and five orbit cases of a 100 m along-track maneuver are shown in Figure 9, and the resulting maneuver trajectories are shown in Figure 11. The primer in the two orbit case satisfies the necessary conditions for optimality, but extrapolating the primer magnitude into the future clearly shows that it is not globally optimal. The same would be seen if the primer magnitude in the five orbit case was extrapolated as well. Note that the (locally) optimal maneuver times are not spaced precisely an integer number of orbits apart because the optimal thrusts have a small radial component as well, as shown in the magnified plots of Figure 11. The fuel cost for the five orbit maneuver is 2.387 mm/s, whereas the cost for a purely tangential five orbit maneuver is 2.4 mm/s. The cost for the two orbit maneuver is 5.967 mm/s.

Out-of-Plane Maneuver—Next, out-of-plane motion is added and a maneuver is designed to reconfigure a formation from a

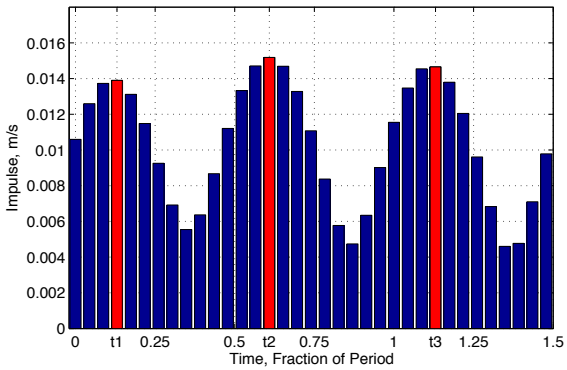

Figure 10. Impulse magnitudes for maneuver to safety ellipse, identifying candidate optimal impulse times.

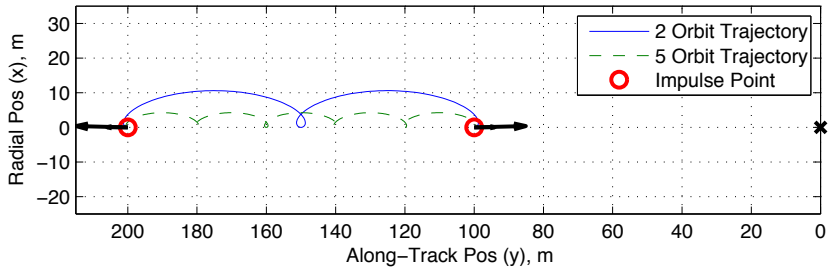

(a) LVLH relative position.

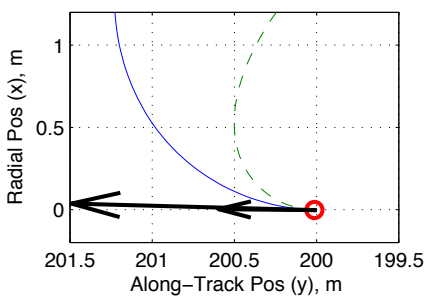

(b) Magnified view of impulse.

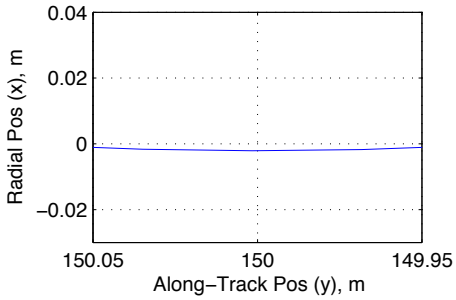

(c) Magnified view of midpoint.

Figure 11. Two and five orbit along-track maneuver, $e = 0$.

$\rho = 200$ m, $\alpha_0 = 0$ in-plane ellipse to a $\rho = 400$ m, $\alpha_0 = \frac{\pi}{4}$, $\rho_z = 200$ m, $\beta_0 = \frac{3\pi}{4}$ safety ellipse, in a circular orbit with J_2 included in the dynamics. An initial estimate for the candidate optimal thrust times is obtained from the discrete-time optimal impulse profile in Figure 10. The iterative refinement of the primer history is shown in Figure 12, which results in a 3-impulse optimal maneuver.

In this case, the optimal primer magnitude is equal to one for the entire maneuver, which is still a valid solution of the degenerate type discussed by Prussing [1]. The optimal thrust times cannot be immediately identified by examining the final primer history, but they are still determined by this algorithm since it converges to the optimal times from a series of compatible suboptimal solutions. The optimal 3-impulse trajectory is shown in Figures 14 and 15 and the total fuel cost for the maneuver is 0.3093 m/s. Using the method of Vaddi et al. [14], the 3-impulse fuel cost is 0.5566 m/s.

Comparison to the Method of Anderson and Schaub— The same maneuver to reconfigure a formation from a $\rho = 200$ m, $\alpha_0 = 0$ in-plane ellipse to a $\rho = 400$ m, $\alpha_0 = \frac{\pi}{4}$, $\rho_z = 200$ m, $\beta_0 = \frac{3\pi}{4}$ safety ellipse is now generated using the method of Anderson and Schaub [20]. That method, which is designed for general formation flying applications including those in the geostationary regime, uses a discretized approximation to generate a near-fuel-optimal impulsive control sequence with impulses applied at equal spacings in true anomaly. The method is applicable in general circular, elliptic, and equatorial orbits, because it uses a set of completely nonsingular elements which does not suffer from the same $i = 0$ singularity as the nearly-nonsingular element set used in this paper.

Using an anomaly discretization of $10°$, the resulting 36-impulse trajectory is shown in Figures 16 (labeled "PVA Trajectory"), along with the optimal 3-impulse trajectory of

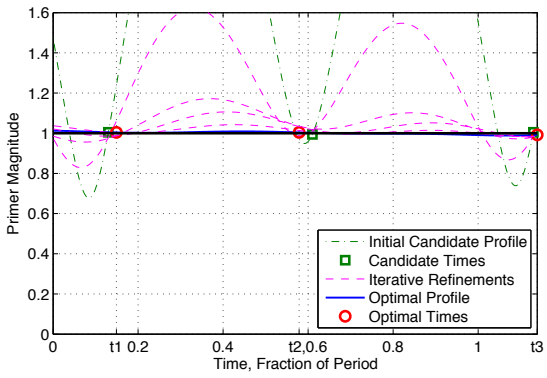

Figure 12. Primer history for maneuver to safety ellipse.

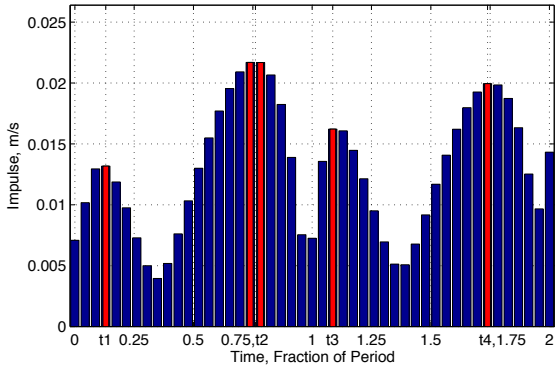

Figure 13. Impulse magnitudes for maneuver to V-Bar, $e = 0.5$, identifying candidate optimal impulse times.

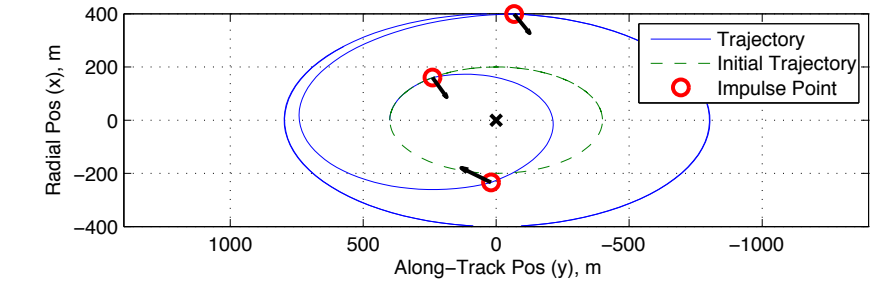

(a) LVLH relative position (in-plane).

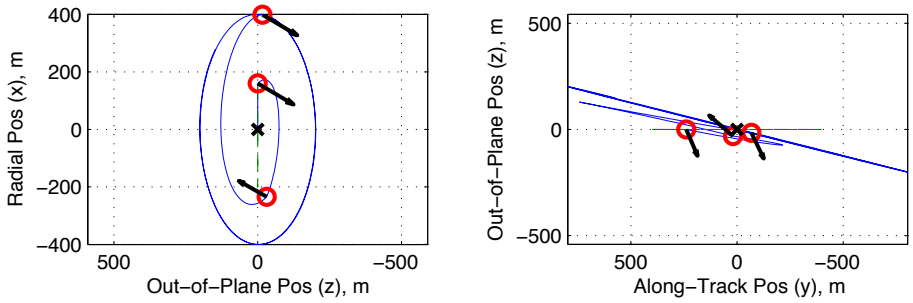

(b) Out-of-plane vs. radial. **(c) Along-track vs. out-of-plane.**

Figure 14. Optimal 3-impulse maneuver to safety ellipse, $e = 0$ with J_2–J_6.

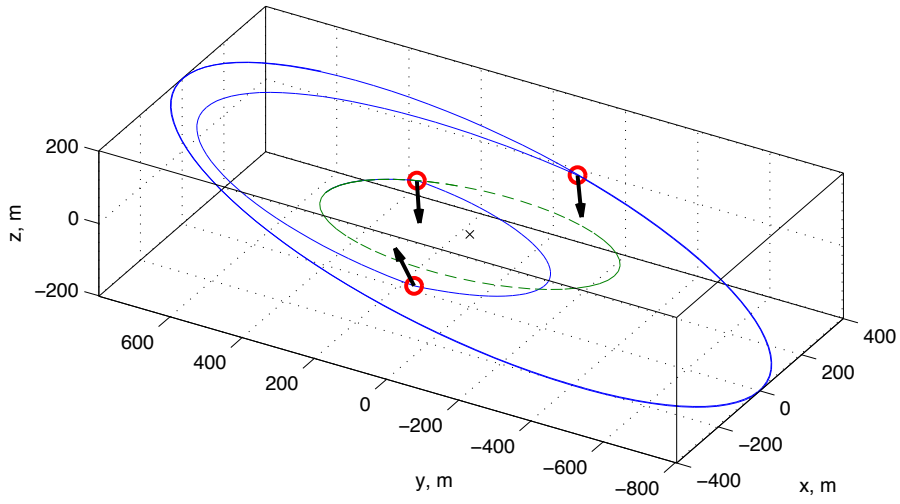

Figure 15. Optimal 3-impulse maneuver to safety ellipse, $e = 0$ with J_2–J_6.

the previous example. In the formulation of Anderson and Schaub [20], the anomaly parameter is not directly controllable, which is the reason for the along-track discrepancy between the two trajectories. The main goal of that method is to reach a formation with a desired size and orientation without specifying a target anomaly. The total fuel cost for the 36-impulse maneuver is 0.3106 m/s, compared to 0.3093 m/s for the optimal 3-impulse maneuver.

Elliptic Orbit

As mentioned previously, the algorithm presented in this paper is also applicable to formations in elliptic reference orbits, with no approximations or loss of fidelity. To demonstrate, the next simulation shows the design of a maneuver in a reference orbit with an eccentricity of $e = 0.5$, from a $\rho = 1$ km, $\alpha_0 = \frac{\pi}{4}$, $\rho_z = 1$ km, $\beta_0 = \frac{3\pi}{4}$ eccentric safety ellipse to a $d = 1$ km average V-Bar position. The actual TH parameters are defined using the eccentric modifications described in Section 2.

An initial estimate for the candidate optimal thrust times is obtained from the discrete-time optimal impulse profile in Figure 13. The iterative refinement of the primer history is shown in Figure 17, which results in the 3-impulse optimal

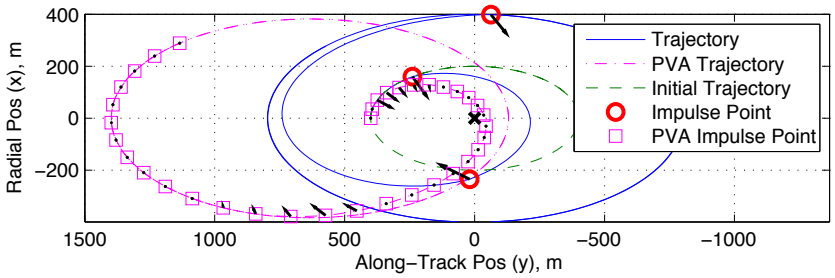

(a) LVLH relative position (in-plane).

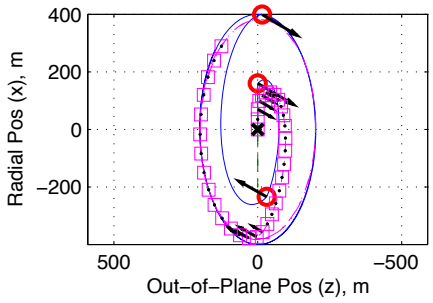

(b) Out-of-plane vs. radial.

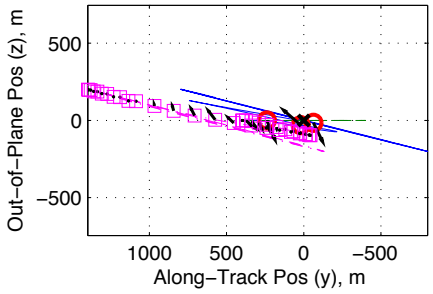

(c) Along-track vs. out-of-plane.

Figure 16. 36-impulse maneuver to safety ellipse compared to optimal 3-impulse maneuver.

maneuver shown in Figures 20 and 21. In this case, the initial candidate maneuver has four impulses, but one is removed during the iterative refinement. In fact, the algorithm initially removed the first impulse but then failed to converge to an optimal primer profile, so the impulse was added back and the final impulse was removed instead. The total fuel cost for the maneuver is 0.4559 m/s.

CPOD Maneuvers in Near-Circular Orbit

The NASA CPOD mission is designed to perform rendezvous, proximity operations, and docking with a pair of identical 3U CubeSats, and is currently scheduled for launch in the fall of 2015. The mission baseline is modeled as a near-circular ($e = 0.005$), 425 km Sun-synchronous orbit. The maneuver targeting algorithm presented here is to be used as the basis of the CPOD guidance system. The mission will employ passively safe trajectories for rendezvous and standby between active operations.

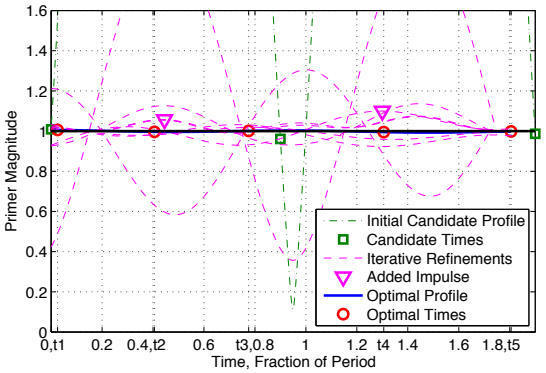

Figure 18. Primer history for CPOD maneuver to initiate walking safety ellipse.

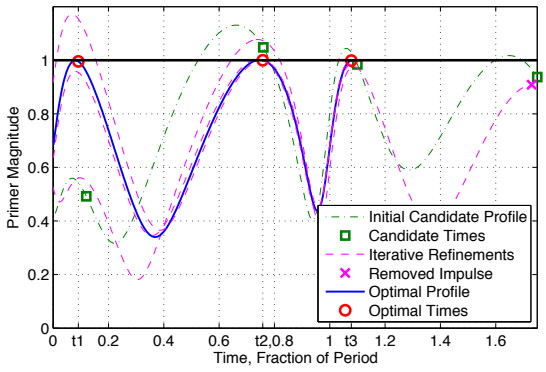

Figure 17. Primer history for maneuver to V-Bar, $e = 0.5$.

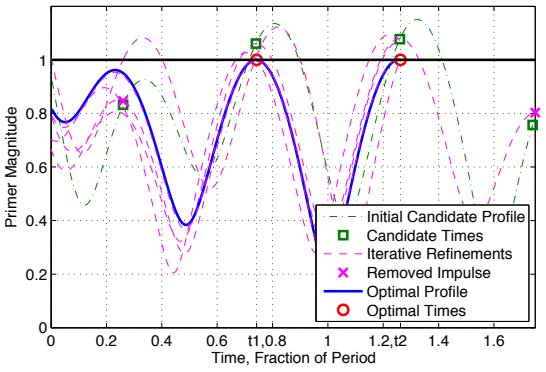

Figure 19. Primer history for CPOD maneuver to safety ellipse.

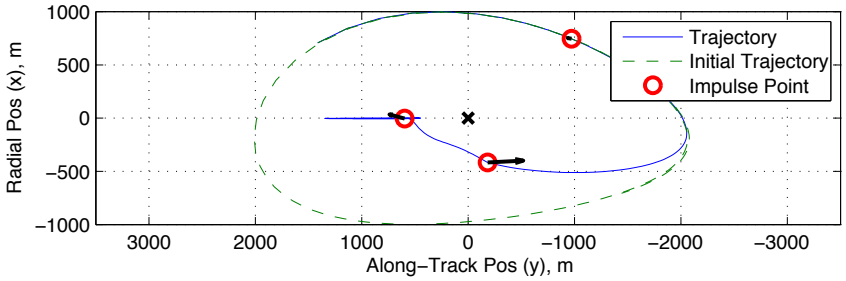

(a) LVLH relative position (in-plane).

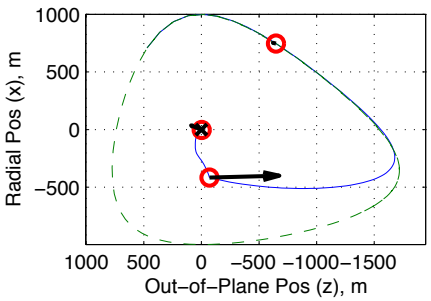

(b) Out-of-plane vs. radial.

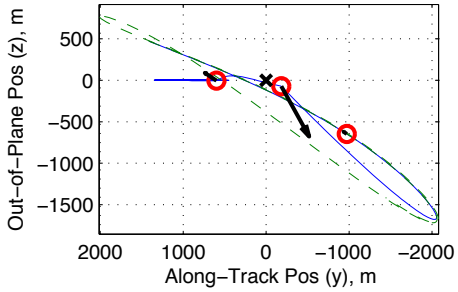

(c) Along-track vs. out-of-plane.

Figure 20. Optimal 3-impulse maneuver to V-Bar, $e = 0.5$ with J_2–J_6.

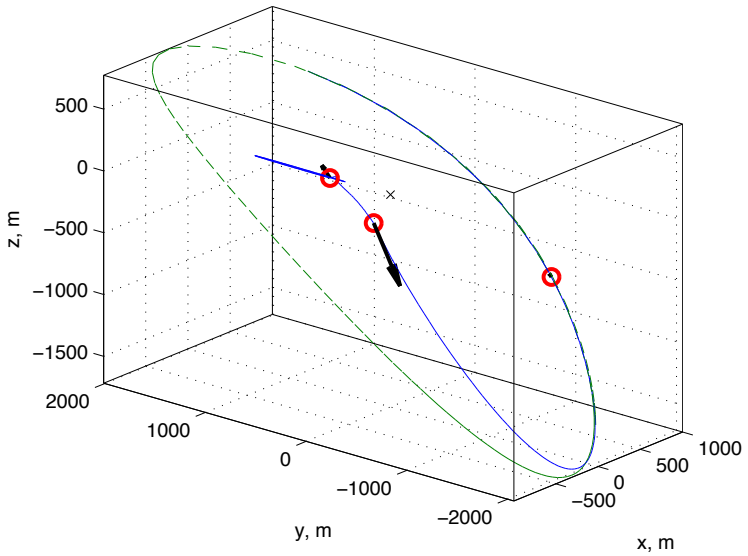

Figure 21. Optimal 3-impulse maneuver to V-Bar, $e = 0.5$ with J_2–J_6.

Initiate Walking Safety Ellipse—The first CPOD maneuver simulated in this section is the initiation of a rendezvous trajectory, i.e. reconfiguring from a safety ellipse displaced some distance away from the chief to a walking safety ellipse. The iterative refinement of the primer history is shown in Figure 18. The initial candidate maneuver has three impulses and two additional impulses are added, resulting in another solution of the degenerate type in which the optimal primer magnitude is equal to one for the entire maneuver. The final 5-impulse optimal maneuver is shown in Figures 22 and 23, and it has a total fuel cost of 23.87 mm/s.

Maneuver to Safety Ellipse—The final maneuver simulated is the initiation of a safety ellipse from a V-Bar standoff position. The iterative refinement of the primer history is shown in Figure 19, which results in a 2-impulse optimal maneuver. This time, the actual trajectory is simulated by applying randomly generated navigation and thrust errors. The initial positions and velocities of the chief and deputy are each displaced by 2 m and 2 mm/s in random directions, and each impulse is applied with 0.5% magnitude and 0.5° direction errors in random orientations.

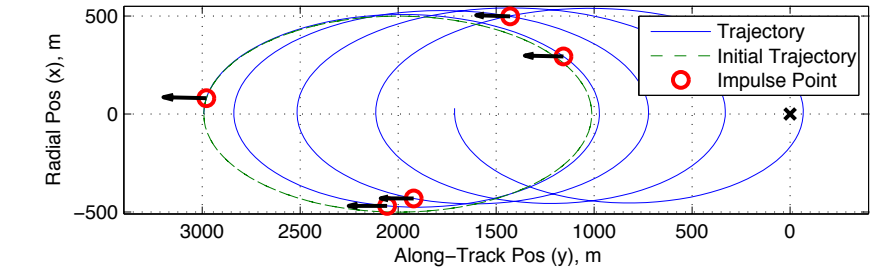

(a) LVLH relative position (in-plane).

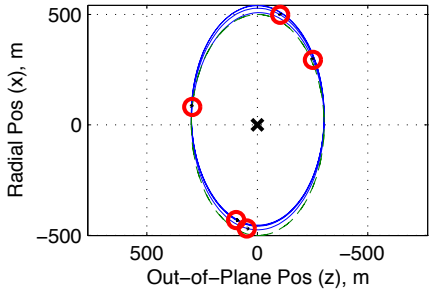

(b) Out-of-plane vs. radial.

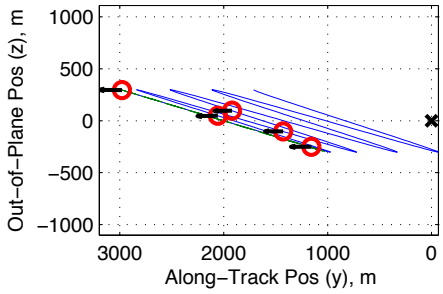

(c) Along-track vs. out-of-plane.

Figure 22. Optimal 5-impulse CPOD maneuver to initiate walking safety ellipse with J_2–J_6.

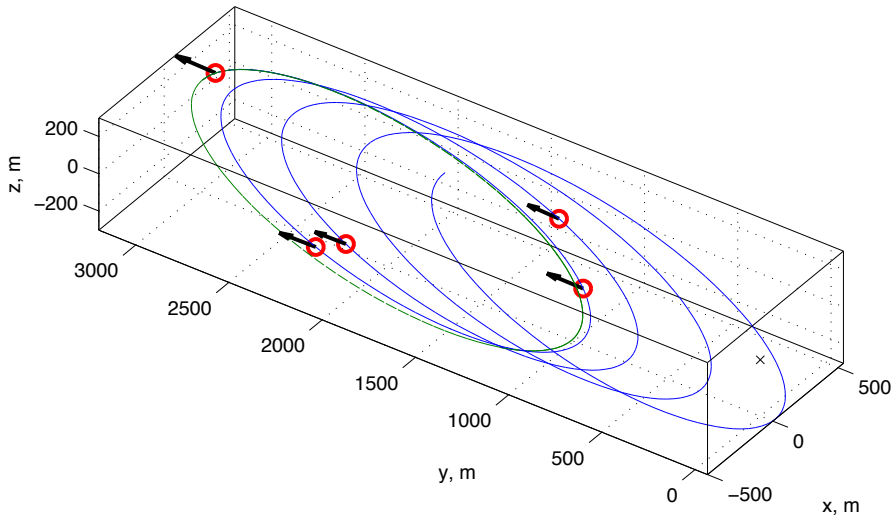

Figure 23. Optimal 5-impulse CPOD maneuver to initiate walking safety ellipse with J_2–J_6.

The resulting 2-impulse optimal maneuver is shown in Figures 24 and 25, where the nominal trajectory shows what the maneuver would look like without errors. As mentioned in Section 1 and described by Carpenter and Alfriend [39], the most significant effect of navigation and thrust errors is unwanted along-track drift cause by differential semimajor axis uncertainty. The total fuel cost for this maneuver is 0.1903 m/s.

6. Conclusions

The dynamic formulation and optimal control equations presented here provide the information necessary to set up the complete formation reconfiguration algorithm derived in this paper. This algorithm is suitable for implementation onboard a spacecraft with limited processing power since it only involves the solution of linear systems, as opposed to more complex methods which require the solution of nonlinear systems. Fuel-optimal, n-impulse reconfiguration maneuvers are designed by iteratively solving a discrete-time maneuver targeting problem, which satisfies the state constraints but does not necessarily use the optimal number of impulses or

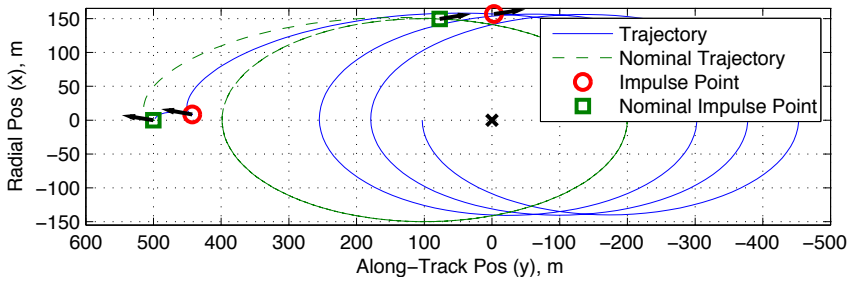

(a) LVLH relative position (in-plane).

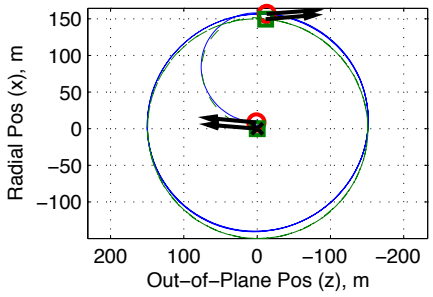

(b) Out-of-plane vs. radial.

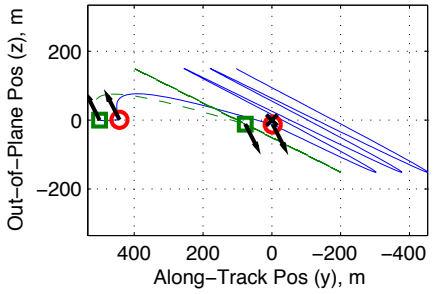

(c) Along-track vs. out-of-plane.

Figure 24. Optimal maneuver to safety ellipse with navigation and thrust errors.

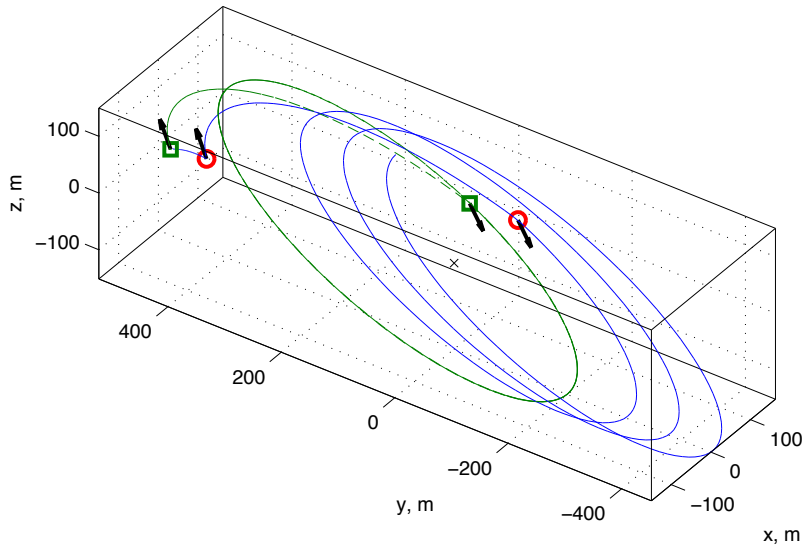

Figure 25. Optimal maneuver to safety ellipse with navigation and thrust errors.

impulse times, using the continuous-time necessary conditions for optimality to refine the impulse times until they converge to the optimal values. Simulation results show that this method, which is uniformly applicable to both circular and elliptic orbits, and includes J_2 effects, produces accurate maneuvers with significantly lower fuel costs than comparable, suboptimal, practically-implementable methods.

ACKNOWLEDGMENTS

The authors wish to thank Scott MacGillivray, Al Tsuda, and John Bowen of Tyvak Nano-Satellite Systems LLC for their support and technical input to this work. Additionally, they thank Paul Anderson of the University of Colorado at Boulder for providing valuable simulation results for comparing this algorithm to the method of Anderson and Schaub [20].

REFERENCES

[1] J. E. Prussing, "Optimal four-impulse fixed-time rendezvous in the vicinity of a circular orbit," *AIAA Journal*, vol. 7, no. 5, pp. 928–935, May 1969.

[2] ——, "Optimal two- and three-impulse fixed-time rendezvous in the vicinity of a circular orbit," *AIAA Journal*, vol. 8, no. 7, pp. 1221–1228, July 1970.

[3] D. J. Jezewski and J. D. Donaldson, "An analytic approach to optimal rendezvous using Clohessy-Wiltshire equations," *Journal of the Astronautical Sciences*, vol. 27, pp. 293–310, July–September 1979.

[4] J. E. Prussing and J.-H. Chiu, "Optimal multiple-impulse time-fixed rendezvous between circular orbits," *Journal of Guidance, Control, and Dynamics*, vol. 9, no. 1, pp. 17–22, January–February 1986.

[5] T. E. Carter and M. Humi, "Fuel-optimal rendezvous near a point in general Keplerian orbit," *Journal of Guidance, Control, and Dynamics*, vol. 10, no. 6, pp. 567–573, November–December 1987.

[6] G. S. Shankar, "An autonomous guidance scheme for orbital rendezvous," Ph.D. Thesis, Indian Institute of Science, Bangalore, India, January 1995.

[7] J. L. Bell, "Primer vector theory in the design of optimal transfers involving libration point orbits," Ph.D. Thesis, Purdue University, West Lafayette, IN, December 1995.

[8] L. H. Mailhe, C. Schiff, and D. Folta, "Initialization of formation flying using primer vector theory," in *International Sympoium on Formation Flying Missions and Technology*, Toulouse, France, October 29–31 2002.

[9] Y.-Z. Luo, J. Zhang, H.-Y. Li, and G.-J. Tang, "Interactive optimization approach for optimal impulsive rendezvous using primer vector and evolutionary algorithms," *Acta Astronautica*, vol. 67, no. 3–4, pp. 396–405, August–September 2010.

[10] B. S. Aubin, "Optimization of relative orbit transfers via particle swarm and primer vector theory," M.S. Thesis, University of Illinois at Urbana-Champaign, Urbana, IL, May 2011.

[11] W. Huang, "Optimal orbit transfers for satellite formation flying applications," Ph.D. Thesis, University of Missouri, Columbia, MO, July 2012.

[12] D. Arzelier, C. Louembet, A. Rondepierre, and M. Kara-Zaitri, "A new mixed iterative algorithm to solve the fuel-optimal linear impulsive rendezvous problem," *Journal of Optimization Theory and Applications*, vol. 159, no. 1, pp. 210–230, October 2013.

[13] Y. Kim, S.-Y. Park, and C. Park, "Semi-analytical global search algorithm for fuel-optimal satellite formation reconfiguration: Impulsive-thrust approach," in *AAS/AIAA Astrodynamics Specialist Conference*, Hilton Head, SC, August 11–15 2013.

[14] S. S. Vaddi, K. T. Alfriend, S. R. Vadali, and P. Sengupta, "Formation establishment and reconfiguration using impulsive control," *Journal of Guidance, Control, and Dynamics*, vol. 28, no. 2, pp. 262–268, March–April 2005.

[15] D. P. Dannemiller, "Multi-maneuver Clohessy-Wiltshire targeting," *Advances in the Astronautical Sciences*, vol. 142, 2011, (Proceedings of the AAS/AIAA Astrodynamics Conference, Girdwood, AK, July 31–August 4 2011).

[16] M. Saunders, "Adaptive formation flying maneuver for multiple relative orbits," M.S. Thesis, University of Colorado, Boulder, CO, August 2011.

[17] L. S. Breger and J. P. How, "Formation flying control for the MMS mission using GVE-based MPC," in *IEEE Conference on Control Applications*, Toronto, Canada, August 28–31 2005.

[18] C. W. T. Roscoe, "Reconfiguration and recovery of formation flying spacecraft in eccentric orbits," M.A.Sc. Thesis, University of Toronto, Toronto, Canada, June 2009.

[19] N. H. Roth, "Navigation and control design for the CanX-4/-5 satellite formation flying mission," M.A.Sc. Thesis, University of Toronto, Toronto, Canada, November 2010.

[20] P. V. Anderson and H. Schaub, "Impulsive feedback control of nonsingular elements in the geostationary regime," in *AIAA/AAS Astrodynamics Specialist Conference and Exhibit*, Minneapolis, MN, August 13–16 2012.

[21] G. Gaias, S. D'Amico, and J.-S. Ardaens, "General multi-impulsive maneuver for optimum spacecraft rendezvous," in *5th International Conference on Spacecraft Formation Flying Missions and Technologies*, Munich, Germany, May 29–31 2013.

[22] D. F. Lawden, *Optimal Trajectories for Space Navigation*. Butterworths, 1963.

[23] C. W. T. Roscoe, J. D. Griesbach, J. J. Westphal, D. R. Hawes, and J. P. Carrico, Jr., "Force modeling and state propagation for navigation and maneuver planning for CubeSat rendezvous, proximity operations, and docking," in *AAS/AIAA Astrodynamics Specialist Conference*, Hilton Head, SC, August 11–15 2013.

[24] K. T. Alfriend and H. Schaub, "Dynamics and control of spacecraft formations: Challenges and some solutions," *Journal of the Astronautical Sciences*, vol. 48, no. 2–3, pp. 249–267, 2000.

[25] K. T. Alfriend and H. Yan, "An orbital elements approach to the nonlinear formation flying problem," in *International Formation Flying Symposium*, Toulouse, France, October 29–31 2002.

[26] H. Schaub, "Relative orbit geometry through classical orbit element differences," *Journal of Guidance, Control, and Dynamics*, vol. 27, no. 5, pp. 839–848, September–October 2004.

[27] P. Sengupta and S. R. Vadali, "Relative motion and the geometry of formations in Keplerian elliptic orbits," *Journal of Guidance, Control, and Dynamics*, vol. 30, no. 4, pp. 953–964, July–August 2007.

[28] D.-W. Gim and K. T. Alfriend, "State transition matrix of relative motion for the perturbed noncircular reference orbit," *Journal of Guidance, Control, and Dynamics*, vol. 26, no. 6, pp. 956–971, November–December 2003.

[29] R. H. Battin, *An Introduction to the Mathematics and Methods of Astrodynamics*. Reston, VA: American Institute of Aeronautics and Astronautics, Inc., 1999.

[30] H. Schaub, S. R. Vadali, J. L. Junkins, and K. T. Alfriend, "Spacecraft formation flying control using mean orbit elements," *Journal of the Astronautical Sciences*, vol. 48, no. 1, pp. 69–87, January–March 2000.

[31] H. Schaub and K. T. Alfriend, "Impulsive feedback control to establish specific mean orbit elements of

spacecraft formations," *Journal of Guidance, Control, and Dynamics*, vol. 24, no. 4, pp. 739–745, July–August 2001.

[32] J.-F. Hamel and J. de Lafontaine, "Linearized dynamics of formation flying spacecraft on a J_2-perturbed elliptical orbit," *Journal of Guidance, Control, and Dynamics*, vol. 30, no. 6, pp. 1649–1658, November–December 2007.

[33] G. W. Hill, "Researches in the lunar theory," *American Journal of Mathematics*, vol. 1, no. 1, pp. 5–26, 1878.

[34] W. H. Clohessy and R. S. Wiltshire, "Terminal guidance system for satellite rendezvous," *Journal of the Aerospace Sciences*, vol. 27, no. 9, pp. 653–658, 1960.

[35] W. Fehse, *Automated Rendezvous and Docking of Spacecraft*. Cambridge, UK: Cambridge University Press, 2003.

[36] D. C. Woffinden, "Angles-only navigation for autonomous orbital rendezvous," Ph.D. Dissertation, Utah State University, Logan, UT, May 2008.

[37] K. T. Alfriend, S. R. Vadali, P. Gurfil, J. P. How, and L. S. Breger, *Spacecraft Formation Flying: Dynamics, Control and Navigation*. Oxford, UK: Elsevier, 2010.

[38] J. Tschauner and P. Hempel, "Rendezvous zu einem in elliptischer bahn umlaufenden ziel," *Astronautica Acta*, vol. 11, no. 5, pp. 312–321, 1965.

[39] J. R. Carpenter and K. T. Alfriend, "Navigation accuracy guidelines for orbital formation flying," in *AIAA Guidance, Navigation, and Control Conference and Exhibit*, Austin, TX, August 11–14 2003.

[40] C. J. Dennehy and J. R. Carpenter, "Demonstration of Autonomous Rendezvous Technology mishap investigation board review," NASA ESC, Tech. Rep. RP-06-119, December 2006.

[41] B. J. Naasz, "Safety ellipse motion with coarse sun angle optimization," in *NASA GSFC Flight Mechanics Symposium*, Greenbelt, MD, October 18–20 2005.

[42] S. D'Amico and O. Montenbruck, "Proximity operations of formation-flying spacecraft using an eccentricity/inclination vector separation," *Journal of Guidance, Control, and Dynamics*, vol. 29, no. 3, pp. 554–563, May–June 2006.

[43] D. E. Gaylor and B. W. Barbee, "Algorithms for safe spacecraft proximity operations," *Advances in the Astronautical Sciences*, vol. 127, 2007, (Proceedings of the 17th AAS/AIAA Space Flight Mechanics Meeting, Sedona, AZ, January 28–February 1 2007).

[44] C. J. Dennehy and J. R. Carpenter, "A summary of the rendezvous, proximity operations, docking, and undocking (RPODU) lessons learned from the Defense Advanced Research Project Agency (DARPA) Orbital Express (OE) demonstration system mission," NASA, Tech. Rep. TM-2011-217088, April 2011.

[45] K. T. Alfriend, H. Schaub, and D.-W. Gim, "Gravitational perturbations, nonlinearity and circular orbit assumption effects on formation flying control strategies," *Advances in the Astronautical Sciences*, vol. 104, pp. 139–158, 2000, (Proceedings of the AAS Guidance and Control Conference, Breckenridge, CO, February 2–6 2000).

[46] D. Brouwer, "Solution of the problem of artificial satellite theory without drag," *The Astronomical Journal*, vol. 64, no. 1274, pp. 378–397, November 1959.

[47] H. Schaub and J. L. Junkins, *Analytical Mechanics of Space Systems*. Reston, VA: American Institute of Aeronautics and Astronautics, Inc., 2003.

[48] K. T. Alfriend and H. Yan, "An evaluation and comparison of relative motion theories," *Journal of Guidance, Control, and Dynamics*, vol. 28, no. 2, pp. 254–263, March–April 2005.

[49] R. G. Melton, "Time-explicit representation of relative motion between elliptical orbits," *Journal of Guidance, Control, and Dynamics*, vol. 23, no. 4, pp. 604–610, July–August 2000.

[50] G. Inalhan, M. Tillerson, and J. P. How, "Relative dynamics and control of spacecraft formations in eccentric orbits," *Journal of Guidance, Control, and Dynamics*, vol. 25, no. 1, pp. 48–59, January–February 2002.

[51] S. S. Vaddi, S. R. Vadali, and K. T. Alfriend, "Formation flying: Accomodating nonlinearity and eccentricity perturbations," *Journal of Guidance, Control, and Dynamics*, vol. 26, no. 2, pp. 214–223, March–April 2003.

[52] S. R. Vadali, S. S. Vaddi, and K. T. Alfriend, "A new concept for controlling formation flying satellite constellations," *Advances in the Astronautical Sciences*, vol. 108, pp. 1631–1648, 2001, (Proceedings of the AAS/AIAA Spaceflight Mechanics Meeting, Santa Barbara, CA, February 11–15 2001).

[53] H. Schaub and K. T. Alfriend, "J_2 invariant reference orbits for spacecraft formations," *Celestial Mechanics and Dynamical Astronomy*, vol. 79, no. 2, pp. 77–95, February 2001.

[54] C. W. T. Roscoe, S. R. Vadali, and K. T. Alfriend, "Design of satellite formations in orbits of high eccentricity with performance constraints specified over a region of interest," *Journal of the Astronautical Sciences*, vol. 59, no. 1–2, pp. 145–164, January–June 2012.

[55] S. F. McAdoo, Jr., D. J. Jezewski, and G. S. Dawkins, "Development of a method for optimal maneuver analysis of complex space missions," NASA, Tech. Rep. TN D-7882, April 1975.

[56] D. J. Jezewski, "Primer vector theory and applications," NASA, Tech. Rep. TR R-454, November 1975.

[57] P. M. Lion and M. Handelsman, "Primer vector on fixed-time impulsive trajectories," *AIAA Journal*, vol. 6, no. 1, pp. 127–132, January 1968.

[58] D. J. Jezewski and H. L. Rozendaal, "An efficient method for calculating optimal free-space n-impulse trajectories," *AIAA Journal*, vol. 6, no. 11, pp. 2160–2165, November 1968.

[59] L. W. Neustadt, "Optimization, a moment problem and nonlinear programming," *SIAM Journal on Control*, vol. 2, pp. 33–53, 1964.

[60] J. E. Potter and R. G. Stern, "Optimization of midcourse velocity corrections," in *Proceedings of the IFAC Symposium on Automatic Control in the Peaceful Uses of Space*, J. A. Aseltine, Ed. New York, NY: Plenum Press, June 1965, pp. 70–84.

BIOGRAPHY

Christopher Roscoe *received bachelor's and master's degrees in Aerospace Engineering from the University of Toronto in 2007 and 2009 and a Ph.D. specializing in spacecraft dynamics and control from Texas A&M University in 2012. He has authored numerous peer-reviewed journal articles and conference proceedings on such topics as spacecraft formation flying, astrodynamics, and space situational awareness. Dr. Roscoe is now an aerospace engineer at Applied Defense Solutions where he performs guidance, navigation, and control analysis for an upcoming CubeSat formation flying mission, as well as astrodynamics research on subjects including track initiation from sparse optical data for space surveillance.*

Jason Westphal *received his B.S. and M.S. degrees in Aerospace Engineering with an emphasis on astrodynamics, control systems, and computer science, from the University of Colorado at Boulder in 1996 and 1998. Mr. Westphal is a Senior Aerospace Engineer at Applied Defense Solutions (ADS), where he is the lead systems engineer for NASA's CubeSat Proximity Operations Demonstration (CPOD) mission. He has over 17 years' experience developing spacecraft Guidance, Navigation, and Control (GN&C) subsystems and flight software. He has been the GN&C lead on programs such as NSPO's FORMOSAT-3, NASA's ST8, and most recently AFRL's ANGELS program, which focused on rendezvous and proximity operations. Prior to joining ADS, Mr. Westphal worked for Orbital Sciences Corporation, the Laboratory for Atmospheric and Space Physics, and the Colorado Center for Astrodynamics Research.*

Jacob Griesbach *received his Bachelor's, Master's, and Ph.D. degrees in Electrical Engineering specializing in adaptive and statistical signal processing from the University of Colorado at Boulder in 1995, 1997, and 2000 respectively. At the MIT Lincoln Laboratory, he contributed key analyses to the space-based radar program. He continued on to provide analyses for space protection studies at the National Reconnaissance Office and the newly founded Space Protection Program office in Colorado Springs. He is now the Technical Director at Applied Defense Solutions, where he is continuing to lead special programs related to space situational awareness. He has over 35 journal and conference publications and is a Senior Member of the IEEE.*

Hanspeter Schaub *received his B.S., M.S. and Ph.D. degrees in Aerospace Engineering from Texas A&M University in 1992, 1994 and 1998. He worked 4 years as a Research Engineer at Sandia National Labs, before spending 4 years at Virginia Tech as an assistant professor. He is currently a professor at the Aerospace Engineering Sciences Department at the University of Colorado at Boulder, and is consulting with Applied Defense Solutions. His research is in nonlinear dynamics and control, spacecraft formation flying, charged astrodynamics, space debris mitigation, as well as attitude control. He has published over 195 conference and journal papers, holds 3 patents, and is the lead author of a popular text book on spacecraft dynamics and control.*

APPENDICES

A. GAUSS'S VARIATIONAL EQUATIONS FOR THE NEARLY-NONSINGULAR ELEMENTS

The nearly-nonsingular form of Gauss's Variational Equations (GVE) is derived from the classical form of Battin [29] using the relationships,

$$e\cos f = q_1\cos\theta + q_2\sin\theta \tag{57}$$
$$e\sin f = q_1\sin\theta - q_2\cos\theta \tag{58}$$
$$\frac{\eta-1}{he} = \frac{-e}{h\left(1+\eta\right)} \tag{59}$$
$$\eta^2 = 1 - q_1^2 - q_2^2 \tag{60}$$

In terms of nearly-nonsingular elements, the orbit equation is

$$r = \frac{a\eta^2}{1+q_1\cos\theta+q_2\sin\theta} \tag{61}$$

The nearly-nonsingular form of GVE is then expressed as

$$\frac{da}{dt} = \frac{2a^2}{h}\left[\left(q_1\sin\theta - q_2\cos\theta\right)u_r + \frac{p}{r}u_t\right] \tag{62}$$
$$\begin{aligned}\frac{d\lambda}{dt} = &\left[\frac{-p}{h\left(1+\eta\right)}\left(q_1\cos\theta+q_2\sin\theta\right) - \frac{2\eta r}{h}\right]u_r \\ &+ \frac{p+r}{h\left(1+\eta\right)}\left(q_1\sin\theta - q_2\cos\theta\right)u_t \\ &- \frac{r\sin\theta\cos i}{h\sin i}u_h\end{aligned} \tag{63}$$
$$\frac{di}{dt} = \frac{r\cos\theta}{h}u_h \tag{64}$$
$$\begin{aligned}\frac{dq_1}{dt} = &\frac{p\sin\theta}{h}u_r + \frac{1}{h}\left[\left(p+r\right)\cos\theta + rq_1\right]u_t \\ &+ \frac{rq_2\sin\theta\cos i}{h\sin i}u_h\end{aligned} \tag{65}$$
$$\begin{aligned}\frac{dq_2}{dt} = &\frac{-p\cos\theta}{h}u_r + \frac{1}{h}\left[\left(p+r\right)\sin\theta + rq_2\right]u_t \\ &- \frac{rq_1\sin\theta\cos i}{h\sin i}u_h\end{aligned} \tag{66}$$
$$\frac{d\Omega}{dt} = \frac{r\sin\theta}{h\sin i}u_h \tag{67}$$

B. Differential Form of Lagrange's Planetary Equations

The Jacobian of the Lagrange's Planetary Equations (LPE) is formed by populating the columns of $\mathbf{A}$ with the partial derivatives with respect to each of the nearly-nonsingular mean elements:

$$\mathbf{A} = [a_{ij}] = \left[\frac{\partial f_i}{\partial \alpha_j}\right] \tag{68}$$

Defining the constant parameter ϵ as in Schaub et al. [30],

$$\epsilon = J_2 \left(\frac{R_e}{p}\right)^2 n \tag{69}$$

the nonzero elements of $\mathbf{A}$ are

$$\frac{\partial f_\lambda}{\partial a} = \frac{-3n}{2a} - \frac{21\epsilon}{8a}\left[\eta\left(3\cos^2 i - 1\right) + \left(5\cos^2 i - 1\right)\right] \tag{70}$$

$$\frac{\partial f_\lambda}{\partial i} = \frac{-3\epsilon}{4}\left(3\eta + 5\right)\sin 2i \tag{71}$$

$$\frac{\partial f_\lambda}{\partial q_1} = \frac{3\epsilon}{4\eta^2}\left[3\eta\left(3\cos^2 i - 1\right) + 4\left(5\cos^2 i - 1\right)\right] q_1 \tag{72}$$

$$\frac{\partial f_\lambda}{\partial q_2} = \frac{3\epsilon}{4\eta^2}\left[3\eta\left(3\cos^2 i - 1\right) + 4\left(5\cos^2 i - 1\right)\right] q_2 \tag{73}$$

$$\frac{\partial f_{q_1}}{\partial a} = \frac{21\epsilon}{8a}\left(5\cos^2 i - 1\right) q_2 \tag{74}$$

$$\frac{\partial f_{q_1}}{\partial i} = \frac{15\epsilon}{4} q_2 \sin 2i \tag{75}$$

$$\frac{\partial f_{q_1}}{\partial q_1} = \frac{-3\epsilon}{\eta^2}\left(5\cos^2 i - 1\right) q_1 q_2 \tag{76}$$

$$\frac{\partial f_{q_1}}{\partial q_2} = \frac{-3\epsilon}{4}\left(1 + \frac{4q_2^2}{\eta^2}\right)\left(5\cos^2 i - 1\right) \tag{77}$$

$$\frac{\partial f_{q_2}}{\partial a} = -\frac{21\epsilon}{8a}\left(5\cos^2 i - 1\right) q_1 \tag{78}$$

$$\frac{\partial f_{q_2}}{\partial i} = \frac{-15\epsilon}{4} q_1 \sin 2i \tag{79}$$

$$\frac{\partial f_{q_2}}{\partial q_1} = \frac{3\epsilon}{4}\left(1 + \frac{4q_1^2}{\eta^2}\right)\left(5\cos^2 i - 1\right) \tag{80}$$

$$\frac{\partial f_{q_2}}{\partial q_2} = \frac{3\epsilon}{\eta^2}\left(5\cos^2 i - 1\right) q_1 q_2 \tag{81}$$

$$\frac{\partial f_\Omega}{\partial a} = \frac{21\epsilon}{4a}\cos i \tag{82}$$

$$\frac{\partial f_\Omega}{\partial i} = \frac{3\epsilon}{2}\sin i \tag{83}$$

$$\frac{\partial f_\Omega}{\partial q_1} = \frac{-6\epsilon}{\eta^2} q_1 \cos i \tag{84}$$

$$\frac{\partial f_\Omega}{\partial q_2} = \frac{-6\epsilon}{\eta^2} q_2 \cos i \tag{85}$$

Note that the only time-varying quantities in this matrix are q_1 and q_2, whose time derivatives are

$$\dot{q_1} = -q_2\dot{\omega} \tag{86}$$

$$\dot{q_2} = q_1\dot{\omega} \tag{87}$$

with

$$\dot{\omega} = \frac{3\epsilon}{4}\left(5\cos^2 i - 1\right) \tag{88}$$

on the order of J_2. The solution to these equations is periodic with a period of $\mathcal{O}\left(J_2^{-1}\right)$,

$$q_1(t) = q_{1,0}\cos\left(\dot{\omega}\left(t - t_0\right)\right) - q_{2,0}\sin\left(\dot{\omega}\left(t - t_0\right)\right) \tag{89}$$

$$q_2(t) = q_{1,0}\sin\left(\dot{\omega}\left(t - t_0\right)\right) + q_{2,0}\cos\left(\dot{\omega}\left(t - t_0\right)\right) \tag{90}$$

where $q_{1,0}$ and $q_{2,0}$ are their values at t_0. Therefore, the matrix $\mathbf{A}$ is composed of only constant and slowly-varying periodic terms.

C. Solution of the Costate Equation

Consider a system of the form

$$\dot{\boldsymbol{x}} = \mathbf{A}(t)\boldsymbol{x} \tag{91}$$

$$\dot{\boldsymbol{\lambda}} = -\mathbf{A}^T(t)\boldsymbol{\lambda} \tag{92}$$

It turns out that

$$\boldsymbol{x}^T(t)\boldsymbol{\lambda}(t) = \text{constant} \tag{93}$$

is an invariant of this dynamical system. To show this, differentiate $\boldsymbol{x}^T\boldsymbol{\lambda}$ and substitute Eqs. (91)–(92) to find

$$\begin{aligned}\frac{\mathrm{d}(\boldsymbol{x}^T\boldsymbol{\lambda})}{\mathrm{d}t} &= \dot{\boldsymbol{x}}^T\boldsymbol{\lambda} + \boldsymbol{x}^T\dot{\boldsymbol{\lambda}} \\ &= \boldsymbol{x}^T\mathbf{A}^T(t)\boldsymbol{\lambda} + \boldsymbol{x}^T\left[-\mathbf{A}^T(t)\boldsymbol{\lambda}\right] \\ &= 0\end{aligned} \tag{94}$$

Next, assume state transition matrices have been developed for both states yielding:

$$\boldsymbol{x}(t_2) = \boldsymbol{\Phi}(t_2, t_1)\boldsymbol{x}(t_1) \tag{95}$$

$$\boldsymbol{\lambda}(t_2) = \boldsymbol{\phi}(t_2, t_1)\boldsymbol{\lambda}(t_1) \tag{96}$$

To find the analytical relationship between the STM $\boldsymbol{\phi}(t_2, t_1)$ and $\boldsymbol{\Phi}(t_2, t_1)$, substitute Eqs. (95)–(96) into the invariant property in Eq. (93).

$$\begin{aligned}\boldsymbol{x}^T(t_1)\boldsymbol{\lambda}(t_1) &= \boldsymbol{x}^T(t_2)\boldsymbol{\lambda}(t_2) \\ &= \boldsymbol{x}^T(t_1)\underbrace{\boldsymbol{\Phi}^T(t_2, t_1)\boldsymbol{\phi}(t_2, t_1)}_{\mathbf{I}_{6\times 6}}\boldsymbol{\lambda}(t_1)\end{aligned} \tag{97}$$

This leads to

$$\mathbf{I}_{6\times 6} = \boldsymbol{\Phi}^T(t_2, t_1)\boldsymbol{\phi}(t_2, t_1) \tag{98}$$

$$\Rightarrow \quad \boldsymbol{\phi}(t_2, t_1) = \boldsymbol{\Phi}^{-T}(t_2, t_1) = \boldsymbol{\Phi}^T(t_1, t_2) \tag{99}$$

Thus, finally, the STM solution of the $\boldsymbol{\lambda}(t)$ trajectory is

$$\boldsymbol{\lambda}(t_2) = \boldsymbol{\Phi}^T(t_1, t_2)\boldsymbol{\lambda}(t_1) \tag{100}$$